Myoelectric Co-Adaptation: Stochastic and Chaotic, yet Describable

by

Ishtar Al-Tahir

Bachelor of Science in Electrical and Computer Engineering, UNB, 2017

A Thesis Submitted in Partial Fulfillment
of the Requirements for the Degree of

Master of Science in Engineering

in the Graduate Academic Unit of Electrical and Computer Engineering

Supervisor:	Erik Scheme, PhD, Electrical and Computer Engineering
	Jon Sensinger, PhD, Electrical and Computer Engineering
Examining Board:	K. Englehart, PhD, Electrical and Computer Engineering
	C.P. Diduch, PhD, Electrical and Computer Engineering
	S. Bateman, PhD, Computer Science

This thesis is accepted by the
Dean of Graduate Studies

THE UNIVERSITY OF NEW BRUNSWICK

March, 2021

ABSTRACT

Myoelectric control systems have advanced over decades, but their performance remains a challenge. Adaptive algorithms have emerged as a possible solution; however, the user is also always learning, causing the resulting system's performance to sometimes be subpar and even unstable. Most studies approximate these co-adaptive systems as combinations of deterministic and stochastic linear systems. Instead, we propose that chaos, a subtype of nonlinear dynamical systems, is required to explain the intermittent performance of myoelectric control systems. Slight, unknown, changes to a chaotic system can shift its dynamics between stable and unstable. In this work, a 10-day co-adaptive myoelectric control experiment was designed to explore this chaotic behaviour. Poincaré mapping, a technique used to visualize chaos, was used to observe how changes to experimental parameters influence the stability of co-adaptive systems and user learning. A better understanding of the dynamics of co-adaptive human-machine interfaces may enable the design and control of more robust systems in the future.

DEDICATION

To mama, baba, and Yona.

ACKNOWLEDGEMENTS

A heartfelt and sincere thank you goes out to my supervisors, Dr. Erik Scheme and Dr. Jon Sensinger. Their patience, support, guidance, and dedication has impacted me throughout my studies and has helped me grow these past few years. Between the research meetings, the personal check-ins, the entrepreneurship support, the shared lunches at the Institute, and tossing a disc on the Ultimate Frisbee field, I couldn't have asked for better mentors.

The IBME is a family and I am lucky to have been a part of it. I must thank Kristel for her encouragement and smiling face around the office, Dr. Biden for his stories during Beers with Biden, and Dr. Kevin Englehart for his encouragement. To the friends I've made at IBME, you have no idea how happy I am to have met you. Thanks for the adventures and countless controls chats we've had, Neil and Anjana, and I hope we have many more. Anjana, thank you for the daily check-ins and the openness to any brain-picking sessions. Extra special thanks goes to Ahmed for his patience and time whenever I messaged in a panic. This thesis could not have been done without you.

To my family, thank you for your continuous love and support. Extra thanks must be said for the endless laughs along the way.

Lastly, to a future Ishtar, if you happen to read this, know that all was well.

Table of Contents

List of Tables

List of Figures

List of Symbols, Nomenclature or Abbreviations

DOF ..... Degree of Freedom

HMI ..... Human-Machine Interface

BCI ..... Brain-Computer Interface

$\overline{AS}$ ..... Non-Adapting, Non-Sparse - used to denote a static algorithm trained using a full complement of training repetitions

$\bar{A}S$ ..... Non-Adapting, Sparse - used to denote a static algorithm trained using a subset of the available training repetitions

$A\bar{S}$ ..... Adapting, Non-Sparse - used to denote an adaptive algorithm trained using a full complement of training repetitions

AS ..... Adapting, Sparse - used to denote an adaptive algorithm trained using a subset of the available training repetitions

PCA ..... Principal Component Analysis

TP ..... Throughput

TPe ..... Effective Throughput

ACE ..... Acquisition and Control Environment

1. Introduction

1.1 Motivation

Decades of research have improved the functionality and usability of myoelectric prostheses, yet user acceptance rates remain low [1]. One requirement for the usability of a prosthesis is that it be intuitive to control and be robust to the natural variability in electromyographic signals (EMG) [1], [2]. Natural changes in myoelectric signals that occur during practical use, however, have been shown to negatively affect the reliability of this control [3]. These challenges to the real-time usage of myoelectric devices include time-varying non-stationarities, user fatigue, changes in limb and electrode positions, and motion artifact [3], [4]. Multiple solutions have been developed to counteract these issues, such as pattern recognition-based control schemes [5], [6], modifying the training stage to strengthen the users' ability to use pattern-recognition control [7]–[9], adapting the control algorithm over time [10], [11], and using augmented feedback [12], [13]. Throughout these studies, a common finding was the importance of incorporating the user in the training process through feedback so they may learn from the machine, whether actively or subconsciously, over time. The pattern-recognition control scheme can then adapt itself during regular use to further improve accuracy. These advancements have culminated in the development of co-adaptive myoelectric control systems.

In co-adaptive control systems, both the user and machine concurrently learn from each other through continuous feedback [14]–[16]. Co-adaptive systems have been used in multiple applications, such as speech and gesture recognition, brain-computer interfaces, and human-machine interfaces such as myoelectric prostheses [17]–[19].

Treating the user and machine as linked subsystems that concurrently adapt has led to more efficient training, reducing user burden while increasing the capacity and speed with which they learn and generalize new strategies. In some cases, the performance and usability of myoelectric systems have also improved with the use of co-adaptive systems [20]. However, delays and disconnects in feedback within the system can lead to instability causing these systems to become unstable and diverge or oscillate away from the target [14], [17]. While signal processing-based approaches have dominated the myoelectric control literature, these co-adaptive systems can be thought of as a set of interacting components within a system that is controlled to reach a desired output, that is, a control system. Consequently, applying knowledge commonly associated with control techniques may lead to a better understanding of the dynamics of co-adaptive Human Machine Interfaces (HMIs).

In this work, we suggest that co-adaptive myoelectric control systems can be further developed if we reframe the way their behaviour is analysed. Existing analytical techniques assume that myoelectric pattern recognition is a mixture of deterministic processes, where the inputs and parameters of a system directly determine its output, and stochastic processes, where inherent randomness affects the output. In reality, however, they may also be chaotic. If so, there is a repertoire of analysis tools that could be used to elucidate patterns of learning and adaptation within chaotic systems. Applying these techniques to myoelectric pattern recognition could explain complex interactions that occur when humans and machines co-adapt during HMI using myoelectric control. However, existing analysis techniques are not robust to the chaotic nature of human-

machine co-adaptive myoelectric systems and neglect to describe key performance attributes when these systems are used over time.

1.2 Objectives

The objective of this work was to describe the possibly chaotic nature of co-adaptive EMG-based HMIs. The knowledge gained by analysing the dynamics of these co-adaptive systems may lead to a better understanding of how to design more robust myoelectric systems. This objective was explored through the following specific aims:

- Specific Aim 1: Develop an experiment to observe and confirm the presence of chaotic behaviour in co-adaptive EMG-based HMIs.
- Specific Aim 2: Evaluate the dynamics of the co-adaptive system through Poincaré maps, a geometrical control technique used to visualize chaos.
- Specific Aim 3: Elucidate trends and distinctions in the behaviour of the system through the developed framework.

2. Background and Related Work

The following chapter reviews recent advancements in myoelectric control, including various algorithms and adaptation schemes. The rationale behind incorporating control theory with co-adaptive systems is substantiated, with a focus on the anticipated chaotic aspect of co-adaptive systems. Finally, the techniques used in this work to control the co-adaptive system and analyse its behaviour are discussed.

2.1 Pattern Recognition-Based Control Schemes

Machine learning techniques have been widely used in myoelectric control to classify EMG signals from the user into a set of actions to control a device. These control strategies have been extensively studied in laboratory and clinical settings, and have recently been commercialized for clinical use [21]. The use of classification strategies has yielded high classification accuracies, especially in offline tasks, but inherently includes several shortcomings. Classification approaches only facilitate sequential control policies (one class or degree of freedom at a time), which limits their effectiveness for simultaneous multifunctional control [22], [23]. Additional classes comprised of combined motions can be added to the training phase to overcome this shortcoming [14], [24], but at the expense of increased training time and complexity, leading to fatigue and frustration for the user. Furthermore, while classification accuracy can be high, the association between offline accuracies and prosthesis usability is weak [22].

2.1.1 Regression

Regression controllers are an alternative to classifiers and are capable of supporting multiple degrees of freedom (DOF) concurrently [25]. Unlike the discrete output of a classifier, a regressor outputs a continuous control value for each DOF and does not decide on one specific class [26]. This method overcomes the drawback of sequential motions in classifiers [3], [26], [27], and instead provides independent, proportional, and simultaneous control of multiple DOFs [26]. Continuous control is also arguably more natural to users, [13], [28], [29], but is less robust to unintentional changes in activation patterns [30]. Nevertheless, the continuous nature of regression-based control inherently incorporates more feedback than discretized classification outputs, enabling users to develop better internal models[1] [30], [31]. Stronger internal models mean that users have an enhanced understanding of their control and are more likely to learn from their device and adapt to any changes. Due to the advantages of simultaneous and continuous control, improved feedback, better formation of internal models, and better user adaptation, regression was chosen for use in this work.

2.1.2 Position Control

EMG control is usually employed in either position or velocity control modes, subject to the constraints of the application. In position control, the intensity of the muscle contraction is directly mapped to the position or orientation of the device through a direct

[1] A person's estimate of the properties of the body and the external world is termed an internal model and is made stronger when more information is acquired [30], [110].

relationship [32]. Alternatively, velocity control proportionally maps the intensity of the muscle contraction to the speed of the output [32]. Velocity control is more often used in clinical prosthetics, and thus research environments, because users do not have to contract to maintain a position [33]–[35]. Velocity control's ability to smoothen EMG signal fluctuations through its derivative method is another advantage over position control [35], but correspondingly abstracts the direct mapping between EMG activation and position which has been shown to provide able-bodied users with more intuitive control and lead to shorter training periods [12], [32], [34], [36]. Position control has additional benefits when combined with regression control schemes, such as providing a higher level of dexterity when controlling multiple DOFs [12] and inherently providing more feedback [30]. Users can better understand their control when provided with a wide range of information through direct feedback of their motions in position control and, therefore, can more readily adapt to changes in the controller. User adaptation is an important factor in the development of effective co-adaptive HMIs, and so position control was chosen for this work.

2.2 Adaptation to Myoelectric Control

2.2.1 Algorithm Adaptation

Pattern recognition-based control schemes, in comparison to conventional myoelectric control schemes, improve the functionality of myoelectric devices [6] over short-term use [5], but environmental changes and changes in the EMG signals over time preclude their long-term use without retraining [38]. Classifiers and regressors rely on repeatable patterns of muscle activity and are therefore confounded by changes due to

donning/doffing, muscle fatigue, electrode shift, and external interferences that may occur during everyday use [4]. Consequently, pattern recognition schemes either require regular retraining [10], [39] or must adapt with the user over time [3], [10], [20], [40], [41]. The need to regularly retrain models introduces added burden and complexity for the user and retraining is likely only initiated once degradation in performance has already occurred. Conversely, adaptive algorithms regularly (or periodically) update their model parameters based on changes in the EMG input to maintain performance without requiring the user to explicitly retrain [10], [16], [42], [43]. Adapting pattern recognition control schemes is challenging, however, due in part to unclear criteria for deciding when and how to adapt [3], [10]. The benefits of adaptive algorithms are worth the challenge, though, as they offer increased reliability to the changes in EMG, leading to improved and prolonged performance [16], [44], [45].

Recent studies have established additional benefits of adaptive algorithms for use with HMIs. Algorithm adaptation can occur in real-time and can combine training data collected offline with online data collected during regular use to build better models. This technique is particularly advantageous when initial training data are limited [40]. The use of static algorithms can lead to a negative effect called overfitting, whereby the machine's learning process is restricted to one specific individual, and any changes in their signals reduces control [23]. Instead, dynamic algorithm adaptation leads to more robust control to changes within and across individuals [46]. When adapting an algorithm, the user's intent (the true motion label) can either be known (or assumed based on some prompt) or unknown, leading to supervised or unsupervised adaptation, respectively [10]. Unsupervised adaptation can be used to account for slow and small changes in EMG

patterns over time and is relatively easy to implement, but an error in the assumed intent can lead to a negative domino effect [10], [23], [47], [48]. Supervised adaptation requires numerous retraining sessions to facilitate labelled data collection, but is more robust to these potential errors [10], [23], [47]. Despite these proposed benefits, further evidence and understanding of the robustness of these dynamical algorithms, especially about how they interact with user learning, is required [3], [10].

2.2.2 User Adaptation

Focusing on adapting the controller alone overlooks the fact that the user is also always adapting with the provision of feedback closing the control loop [49]–[53]. During online myoelectric control, users receive continuous feedback on their commands and can adapt to the changed signal features and learn to counteract the non-stationarities [13]. All users naturally adapt to their myoelectric control, regardless of their initial skill with the control scheme [54], [55]. Humans have an instinctive ability to form internal models [56], [57], optimize control strategies [58], and learn new muscle synergies [59] while completing physical tasks as part of a real-time closed-loop system [60]. Including the user in the loop via feedback, such as inherent visual biofeedback [61], during the training stage promotes a stronger understanding between the user and their myoelectric control system [13], [31]. This understanding is strengthened by a user's ability to correct variations and adapt to user- and algorithm-related errors in real-time [23], [41]. The concurrent learning process between user and machine has a significant impact on the performance of the system [15], [18], [43], [60], [62].

User adaptation is constant in HMIs and Brain Computer Interfaces (BCIs) but knowledge of its role in the behaviour of these systems is limited [15], [19]. Studies are beginning to focus on the human aspect of HMIs to determine how internal models are developed [63] and how their adaptation can be factored into the system design [64]. Researchers have also determined a need to establish metrics that can better describe a user's skill in the use of HMIs [19]. One such metric is the Transfer Index which quantifies user learning and has been used to demonstrate knowledge transfer between similar tasks through the generalization of knowledge [65], [66]. All these studies show that user adaptation is key to a successful HMI but it is not enough to combat the deterioration of EMG signals in myoelectric control [15]. Rather, a complementary combination of machine adaptation and user adaptation is required to balance the system [67]. Indeed, recent research has proposed models that consider the push and pull of information between both the user and machine as they work towards achieving optimal performance [17], [68].

2.2.3 Co-Adaptation

Due to the improved results that have been observed when control algorithms and users adapt, researchers have combined both subsystems into co-adaptive environments. BCIs [40], [69], [70] and HMIs [18], [42], [71] have both benefited from co-adaptive control schemes by enabling the user and machine to learn concurrently in real-time. Co-adaptation can be particularly useful when implemented during the training stage of a myoelectric prosthesis as both user and machine learn to converge to a synergistic strategy more readily [14], [42]. Users who were previously unable to control their BCI have been

able to do so when the adaptation of the machine and user are considered [11], [69]. The user and the machine are then set within a periodic process of adapting and retraining. This amalgamation of user-in-the-loop adaptation and machine learning is thought to improve control and performance in myoelectric devices but the robustness and stability of this dual-learner framework remain underrepresented in the research literature [14], [15], [17], [72].

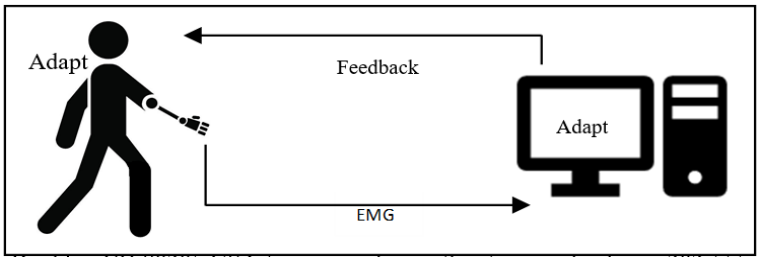

Figure 2-1: Human-Myoelectric-Machine Co-Adaption Flowchart

In the dual-learner framework portrayed in Fig. 2-1, each learner is modelled as a subsystem that works with and responds to the changes of the other learner, creating a dynamic control system. These concurrently learning subsystems aim to generate an optimal solution [43] and, in principle, both converge towards a common control strategy [73] by repeating the adapting and retraining processes periodically. Although this concept is theoretically sound, results from practical applications disagree. Adequate control for research applications can be achieved in co-adaptive systems like HMIs and BCIs, but their practical use has been restricted by their control instability and suboptimal performance [14], [17], [20]. The lack of understanding about the reason for the instability and the uncertainty about the behaviour of the dual-learner framework have impeded its progress.

2.3 Control Theory

An overarching theme in many related studies is that there is an inadequate understanding of the dynamics of adaptation and what constitutes robustness and optimal performance in adaptive systems [3], [10], [17]. While the field of myoelectric control has largely maintained a signal processing perspective on these issues, the analysis of dynamics and optimal performance of such systems is founded in control theory. Exploiting controls-based attributes of co-adaptive systems, such as their periodicity as they loop between an adapting phase and a training phase, may provide additional information that could be used to further analyse and control these systems. BCI research has begun to apply control theories to co-adaptive systems to develop better models and help learn how to enhance the performance of co-adaptive systems [63], [74], [75]. A co-adaptive HMI can be modelled as a 4^{th} order system with two subsystems that are periodically updated by the input and output control signals (Fig. 2-1).

The system's high order is caused by the human and machine's dependency on their past states through a time-step delay, requiring second-order dynamics to describe each subsystem. The nonlinearity of the system stems from the dependency of the human's state on the machine state and vice versa, causing the gains of each subsystem to be dependent on the other. This model is contrary to existing studies that do not take into account the time-delayed human and machine states and instead assume a 2^{nd} order linear model for the co-adaptive system [17], [74]. In an HMI model, the isolated machine can be classified as deterministic because the same set of inputs will produce the same set of outputs. The human also attempts to produce the same output for a given set of inputs, however, the output is always corrupted by noise [17] and is therefore classified as a

stochastic process. Existing works, therefore, have assumed that co-adaptive systems are a combination of deterministic and stochastic, but neglect that the system is nonlinear, periodic (due to its update in states at discrete time-steps), and higher than 3rd order. Taking these factors into consideration suggests that these systems are not only stochastic and deterministic, but possibly also chaotic [76].

Chaos in dynamic systems may manifest as a seemingly random state of disorder but is a deterministically-led process that is sensitive to changes in the initial conditions of the system. It was a mathematician named Lorenz who first established the theory of chaos while trying to model weather [77]. Meteorology is deemed chaotic as it can never practically be 100% confident due to an almost infinite number of internal or external parameters that can change and affect the weather and its forecast [78]. The game of roulette is another real-world system that exhibits chaos; a player may develop an intuition about where the ball will land based on their past participation and bet on that certain play, only to have their "luck" run out when the ball lands on a different tile. This change from presumed knowledge of the endpoint to an unpredicted roll has been attributed to "luck" but is actually the shifting of states from stable to unstable equilibrium points in a chaotic system, dependent on initial conditions such as the speed of the wheel spin or the force of the ball drop. Chaos presents itself in many such real-world applications and this work evaluates its presence in co-adaptive HMIs.

The possibility of chaos in co-adaptive systems arises from their structure and operation. Each subsystem in a co-adaptive myoelectric HMI is a 2nd order system. As these systems' dynamics interact with each other in a feedback loop, a unique system that exhibits higher-order dynamics is created. Additionally, the interaction of human and

machine subsystems necessitates the dependency of one on the other. The control of each learner (gain) is based on the output variables of the other learner, which is dependent yet again on the gain of the subsystem. Given that the states of the system are dependent on other states of the system, the co-adaptive system is inherently nonlinear (see Equations (1) and (2)). The co-adaptive system then advances at fixed interval time steps using the information output from the previous interval, causing the system to be periodic. The combination of these factors leads to the possibility of chaos, making the deterministic HMI more susceptible to initial conditions and increasing the difficulty of long-term prediction [76]. A mathematical technique that can take advantage of these factors to assess the stability of these chaotic systems is therefore needed to better control co-adaptive HMIs.

$$\boldsymbol{gain_1 = f_1(parameters_1, output_2)} \quad \textbf{(1)}$$

$$\boldsymbol{gain_2 = f_2(parameters_2, output_1)} \quad \textbf{(2)}$$

Where the output of each subsystem is dependent on the gain of the other subsystem, as in Equation (3) and (4).

$$\boldsymbol{output_1 = g_1(parameters_1, gain_1)} \quad \textbf{(3)}$$

$$\boldsymbol{output_2 = g_2(parameters_2, gain_2)} \quad \textbf{(4)}$$

2.3.1 Poincaré Maps

Although there are many possible tools with which to analyse chaotic systems [76], a simple yet effective method is through Poincaré mapping. This technique is quantitative-visual and the shape of the map can be used to assess the stability of a system

[76], [79]. Poincaré maps plot the intersection of a periodic orbit with a lower-dimensional, transversal surface, called a Poincaré section [80]. Poincaré maps can be thought of as “next return maps” as they are used to calculate the next trajectory of a system given its previous intersection with the Poincaré section [81]. This visualization tool is a valuable analysis technique due to its ability to display nonlinearity in sequential data [79]. It can describe the approximate behaviour of the dynamics of a system in a lower dimension and can do this without the knowledge of the system’s dynamic equations [82].

Poincaré maps take advantage of the periodicity of systems to analyse their stability and demonstrate any chaotic effects. If the intersection of the periodic orbit with the Poincaré section occurs at the same location over fixed time intervals, then the system’s orbit is stable [83], [84]. Conversely, if the deterministic system displays aperiodic behaviour that is dependent on initial conditions and changes in states, then it exhibits chaos [76]. A Poincaré map can be used to visualize this aperiodicity, making it a useful tool for chaotic system analysis. Fig. 2-2 shows a trajectory intersecting a Poincaré section. The location of trajectory points at each step interval (e.g. x_1) is then plotted against its previous location (e.g. x_0). A Poincaré plot of the progression of each periodic interval’s intersection points can provide information about the system’s stability and may elucidate any chaotic behaviour in the system.

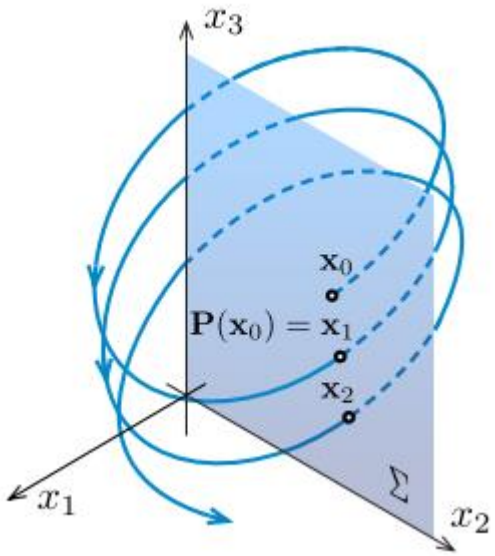

Figure 2-2: System trajectory intersecting a Poincaré section (Σ) at points x_0, x_1, and x_2 over fixed time intervals [85]

Poincaré maps have been used in biomedical research to analyse gait, electroencephalograms (EEG), electrooculograms (EOG), electrohysterogram (EHG), and signal changes in EMG, but are mainly used in measuring heart rate variability in electrocardiograms (ECG) [79], [82], [86]–[88]. In this work, Poincaré maps are used to analyse the proposed chaotic nature of co-adaptive myoelectric systems over time and explore how their dynamics behave as different experimental parameters are varied.

3. Method and Experimental Procedure

The choice of the control scheme, adaptation method, and visualization tool made in this work are all motivated by the goal of identifying chaotic behaviours in co-adaptive human-machine control. A supervised EMG-based regression control scheme, Support Vector Regression (SVR[2]), is used to control a screen-based cursor in a closed-loop experiment. Position control is used to improve the interpretability of feedback and foster the development of strong internal models. In this work, we propose that the resulting co-adaptive system is chaotic, and results are therefore investigated using Poincaré maps, an analytic technique used in high-order, nonlinear systems.

3.1 Data Collection

We explored these ideas in a series of three longitudinal case studies (all female, right-handed, ages 35 ± 18 years) with varying levels of myoelectric control experience to evaluate their performance with a co-adaptive myoelectric control system. The implications of the world-wide COVID-19 pandemic affected the sample number of this experiment, but allowed for a more in-depth, longitudinal study. Before they participated in this experiment, Subject 1 (S1) reported having no experience, Subject 2 (S2) had moderate, and Subject 3 (S3) had extensive experience with myoelectric control. Subjects provided informed consent as approved by the UNB Research Ethics Board (REB #2020-

[2] Support Vector Regression (SVR) is a supervised pattern recognition algorithm that has shown superior performance in Fitts' law metrics and processing speed during real-time control of simultaneous and proportional myoelectric control of multiple DOFs [35], [111].

021). Data were collected from each subject over 40 sessions spread across 10 different days to capture changes in control behaviour over time [89]. Each day consisted of four sessions that lasted approximately 40 minutes each. Eight Delsys Trigno sensors with 2 kHz sampling frequency were attached equidistantly around the user's dominant forearm, at approximately one-third the length of the forearm, distal to the elbow. The user then placed their arm in a plexiglass brace that constrained their forearm and wrist to ensure wrist contractions were isometric. Throughout the experiment, the user performed wrist extension, wrist flexion, wrist abduction, and wrist adduction contractions to train the model and control a cursor on a screen during a target reaching task.

3.1.1 Experimental Setup

Each session consisted of 16 Fitts' Law-style target acquisition sets [90], [91] over three stages - 4 Baseline sets, 10 Feedback-Enabled sets, and 2 Testing sets - as shown in Fig. 3-1. The first stage was used for training and provided no feedback to the user as they were performing the prompted target-reaching tasks. Data from the first stage was used to train the controller for the second and third stages, where feedback was provided.

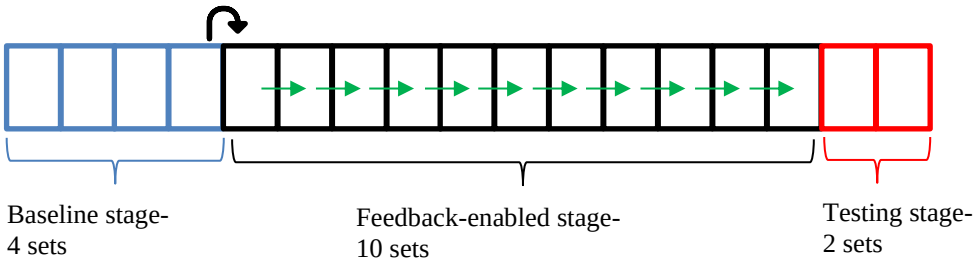

Figure 3-1: Protocol layout explaining number of sets in each stage; black arrow represents regressor training while green arrows represent regressor adaptation if protocol condition required it.

Each set presented 20 targets to the user who then performed wrist contractions with intensities corresponding to the distance from the origin to the prompted target (see Fig. 3-2). These targets were square with a fixed width of 15 units and were located either on the x or y-axis and at one of five different positions, ranging from 0 to 100 units away from the origin. For the furthest target, the user was asked to elicit the maximum wrist contraction intensity that they would be comfortable sustaining throughout the full session, known as the Maximum Voluntary Contraction (MVC). During the Baseline stage, users were asked to elicit contraction levels consistent with 0%, 10%, 20%, 30%, and 40% of their MVC to reach targets located at the 0, 20, 40, 60, and 80 position marks on the positive and negative x and y axes. In this stage, the user performed wrist contractions with the assumption that their intensities were accurate and repeatable enough to reach the target across multiple sets.

These 20 target-reaching tasks were repeated for 4 sets after which a model was trained. The subsequent Feedback-Enabled and Testing stages employed targets located at the 0, 25, 50, 75, and 100 position marks, which corresponded to the contractions of 0%, 25%, 50%, 75%, and 100% of the user's MVC (Fig. 3-2). The 20 targets in each set were presented to the user in a randomized order to promote active thinking and reduce possible learning effects arising from muscle memory. Data from the final two stages were used to test the performance of the co-adaptive system.

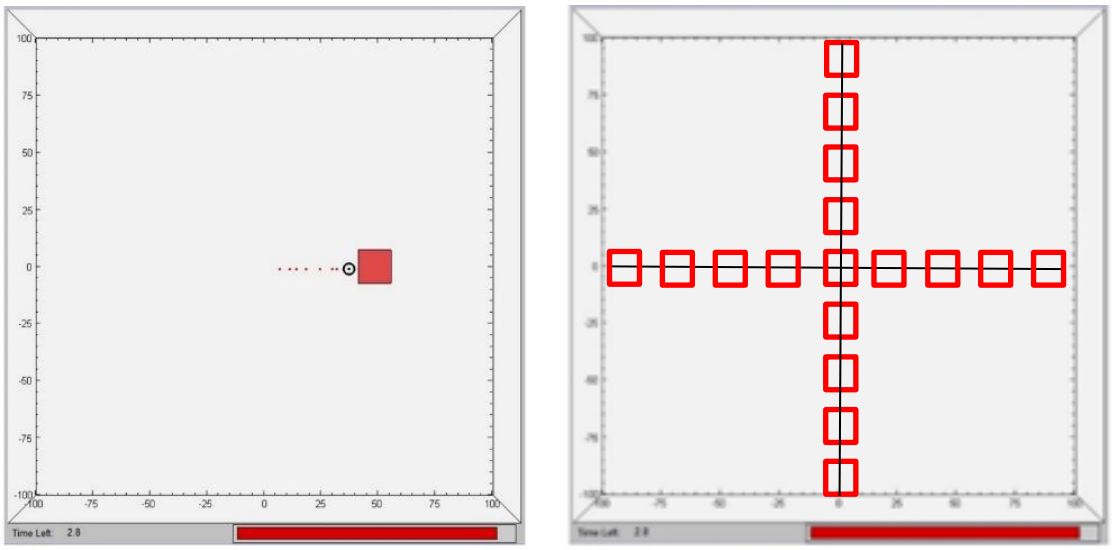

Figure 3-2: Left: Screenshot of the Fitts' Law Environment interface during the Feedback-Enabled stage. The black circular cursor is reaching from the centre of the screen towards the square target positioned at the 50% mark (for this specific example). The path that the cursor takes is displayed in real-time to the user as a red trail.

Right: All possible target locations in the Feedback-Enabled and testing stages overlaid on the Fitts' screen, corresponding with 0%, 25%, 50%, 75%, and 100% MVC on the positive and negative x and y axes.

3.1.2 Experimental Protocol Variations

Two independent experimental parameters - the extent of machine adaptation and the amount of data used in training the algorithm - were varied to produce four combinations of the experimental protocol, as described in Table 1. Combinations of adapting (A) and non-adapting ($\bar{A}$), with a limited (or sparsely-trained, S) or a fully informed (non-sparsely-trained, $\bar{S}$) algorithm were evaluated. These comparisons explored whether changes in the control scheme can affect user learning and the overall stability of the user-machine interaction.

The non-sparsely trained algorithm, $\bar{S}$, used the full dataset collected from the user whereas the sparsely-trained algorithm, S, only used data collected when the user was at

rest position and the maximum distance target. Both the adapting and non-adapting systems, A and $\bar{A}$, respectively, trained an initial regressor using data collected during the baseline stage. During the adapting sessions, AS or $A\bar{S}$, however, the regressor was cleared, retrained, and updated after each target acquisition set during the Feedback-Enabled stage, using only the data collected from the set the user had just performed. Therefore, the user was unknowingly presented with a new controller at each set in the Feedback-Enabled stage when the system was adapting. This process was done to facilitate the comparison of two extremes of adaption – no adaptation at all, vs a complete retraining of the regressor.

It should be noted that two of the three subjects were unaware of this adaptation procedure and were simply given instructions to perform 12 Feedback-Enabled sets after the initial four baseline sets. The third subject was the first author of this work and, therefore, knew the experimental design and session type. The order of sessions was randomized each day and individually for each subject to avoid user bias towards any particular algorithm combination.

Table 3-1: Labels used for the four session types evaluated in the experiment based on the two-parameter changes chosen for this experiment.

	Full Adaptation (A)	**No Adaptation ($\bar{A}$)**
Sparse Training (S)	AS	$\bar{A}S$
Non-sparse training ($\bar{S}$)	$A\bar{S}$	$\overline{AS}$

Subjects began every set with their wrist relaxed and, correspondingly, with the cursor near the centre of the screen. In the baseline stage, during the one-second intervals before a target was displayed, a grey square marker was placed in the position of the upcoming target to inform users of their next action. As all subjects were right-handed, positive and negative targets on the x-axis related to wrist extension and wrist flexion, respectively, while targets on the y-axis required wrist abduction (positive) and wrist adduction (negative). Once the trial began, the target became red and the user had 3 seconds to elicit and maintain a wrist contraction consistent with the target position. The user was then instructed to rest, returning the cursor to the centre of the screen for one second between targets. During this second, the upcoming target was once again revealed by a grey square. These target-reaching tasks were repeated for the 20 trials in each baseline set. This concept was replicated in the Feedback-Enabled and testing stages, but no information about the upcoming target position was provided to the user. Instead, the user saw their cursor move in real-time as they altered their wrist contractions to reach the target position. The target changed colour from red to green if the subject managed to place the cursor in the target successfully. Subjects were made aware of the length of time remaining in each trial by a countdown bar at the bottom of the screen (Fig. 3-2).

Data collected during the baseline stage were used to train the regressor that controlled the cursor in all subsequent sets of the non-adapting protocol variations ($\bar{A}S$ and $\overline{AS}$) and the first set of the Feedback-Enabled stage of the adapting protocol variations (AS and $A\bar{S}$). The first of the four sets collected in the baseline stage was discarded to reduce the impact of learning the protocol during the first set. From the remaining three baseline repetitions, the two that yielded the highest correlation with the sequence of

targets were used to train the regressor. As shown in Fig. 3.3, the user's elicited position data (shown by the black signal) were compared to the intended target positions (shown in red), and the coefficient of determination (R^2) was calculated between the two sequences. This was repeated for each DOF, because a separate SVR was trained to control motions in the x and y axes, referred to as DOF 1 and DOF 2, respectively. In the adapting protocol variations (AS and $A\bar{S}$), each of these regressors was updated after each set in the Feedback-Enabled stage but not after the 10th Feedback-Enabled set, so that the user had some experience with the final controller before the testing stage.

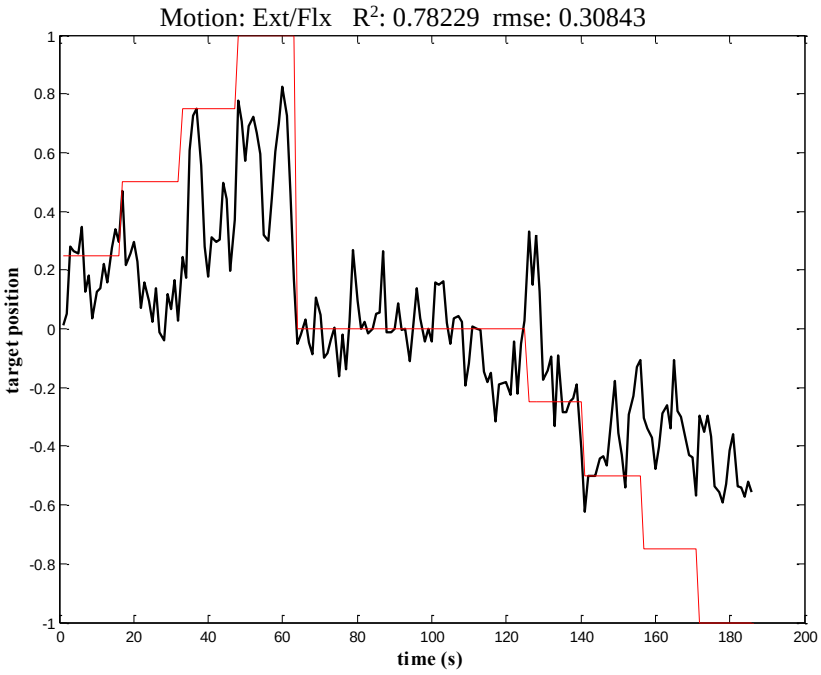

Figure 3-3: Comparing the ideal target position to the obtained user position using R^2, using an example subject's DOF 1 performance.

3.1.3 Signal Processing

The software used to conduct the experiments was an extension of the custom-built University of New Brunswick Acquisition and Control Environment (ACE) program in MATLAB® [92]. Data from the EMG signals were notch filtered with a third-order Butterworth filter to remove powerline noise at 60 Hz, 180 Hz, and 300 Hz. Five common time-domain features - Mean Absolute Value, Wilson's Amplitude, Slope Change, Waveform Length, and Zero Crossings [6], [93] - were extracted from overlapping windows of 320ms (with 128ms increments) and used to train the SVRs [94], [95].

The SVRs were implemented using the LIBSVM codebook [30], giving users control over both DOFs simultaneously and independently, although users were only required to intentionally activate one DOF at a time to reach any given target. A 1€ filter [96] was applied during the Feedback-Enabled and testing stages to reduce the amount of noise inherent in EMG-based position control. A 1€ filter is an adaptive form of a low-pass filter whose cut-off frequency changes to ensure smooth cursor movements regardless of the speed of control. The filter cut-off is dynamically raised during rapid motions to ensure responsiveness but dropped during slow motions to emphasize smoothness.

Additional position gains were applied to the cursor control to ensure that the user's max intensity coincided with the boundaries of the GUI. Data from each session's baseline stage was used to calculate the position gains for each DOF and the position gains were not changed throughout the experiment to reduce the number of adapting elements that may affect learning. These measures were taken to provide comfortable and intuitive position control to the user.

3.2 Observing Performance Metrics

The following section outlines the various performance metrics used in this work.

3.2.1 Conventional Method

EMG data are commonly collected from a given user over a period of time and may represent the muscle signals from multiple actions. Simple time series visualization of metrics extracted from these signals is common when analysing changes over time. Consequently, in this work, time series plots of data over the 10-day experiment are used as a baseline visualization technique.

3.2.2 Poincaré Maps

3.2.2.1 Overview

Typical myoelectric-control metrics are commonly used to measure changes in signal patterns and features of EMG but are computed in isolation and neglect how the dynamics of the human-machine control loop change with adaptation. Poincaré maps can be used to analyse the stability of a system by focusing on the periodicity of its dynamics. The co-adaptive HMI system in this work is periodic because the user and machine adapt and retrain at every set of the training and testing phase. However, a lack of periodicity in the co-adaptive system's observed results due to changes in initial conditions or state parameters can be used as an indication of chaos. Poincaré maps capitalise on this phenomenon and provide information on a system's dynamics that may not be detected using traditional time series methods [97].

A Poincaré map of a system orbit uses a Poincaré section, which is a lower-dimension plane transverse to the flow of the orbit trajectory, as seen in Fig. 3-4. The intersection of this periodic trajectory with the Poincaré section is plotted against its previous intersection to form a Poincaré map. In other words, if $\{\mathbf{y}_1, \mathbf{y}_2, \mathbf{y}_3, ...\}$ is the set of intersections of a trajectory with the surface of a section, then the Poincaré map can be defined by Equation (5) [81]. Poincaré maps are useful for analyzing the dynamics of a periodic system to describe its chaotic nature by looking at the progression of trajectories and determining its stability from the shape of these plots. In this work, Poincaré maps will be used to assess the stability of co-adaptive HMI systems as they perform an iterative Fitts' law-style target acquisition framework.

$$\boldsymbol{P(y_n) = y_{n+1}} \tag{5}$$

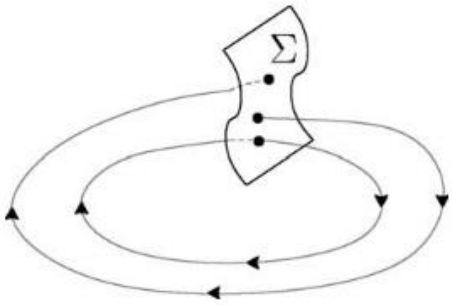

Figure 3-4: Periodic orbit intersecting the planar surface Σ [98]

3.2.2.2 Poincaré Map Behaviours

To provide context for how system dynamics are affected when the human-machine system adapts, a set of reference graphs was created based on how typical Poincaré maps behave for a range of systems (Table 3-3). Without noise and inherent randomness, the behaviour of these systems would be deterministic, as represented by the left column of

Poincaré plots in Table 3-3. However, EMG is stochastic and variability in the signals affects the behaviour of the Poincaré maps, as represented by the rightmost column. The initial conditions used in the models that generated these examples, the length of time the Matlab differential equation solver ran for and the time-steps chosen for the solver, affect the Poincaré map. A Poincaré surface of *x=0* (the *yz* plane) was used to determine the intersection of the trajectory of the simulated examples. These intersection points are mapped to themselves at shifted time-steps (n vs n-1), forming the Poincaré maps of the example systems in Table 3-3.

Table 3-2: Examples of Poincaré maps for a variety of dynamical systems. In the figures, the red y=x line represents the unity line and the '1' represents the starting point of the trajectory.

Type	Equation	Deterministic	Stochastic
Stable	$\dot{x}_1 = x_2$ $\dot{x}_2 = -\frac{b}{ml^2}x_2 - \frac{g}{l}\sin(x_1)$ *where m=6, b=65.01,* *g=9.81, and l=1*	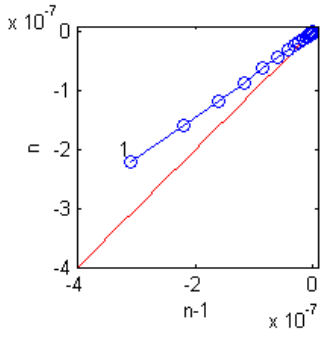	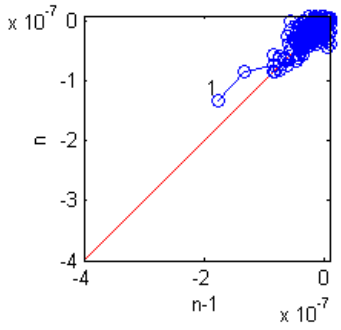
Unstable	$\dot{x}_1 = x_2$ $\dot{x}_2 = x_2^{\frac{1}{5}} - x_1^3$	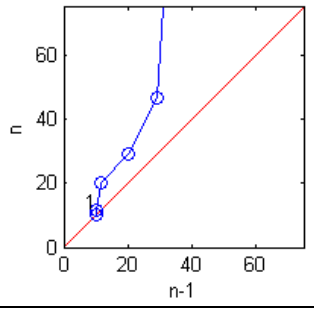	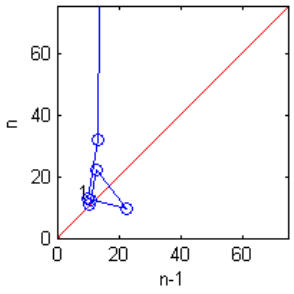

Oscillatory	$\dot{x}_1 = -x_2 - x_3$ $\dot{x}_2 = x_1 + dx_2$ $\dot{x}_3 = d + x_3(x_1 - c)$ *where c=4.16 and d=0.2*	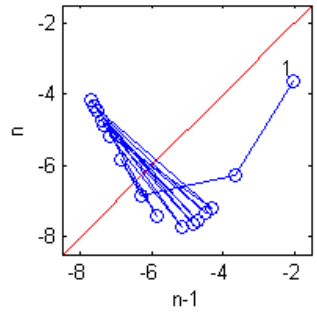	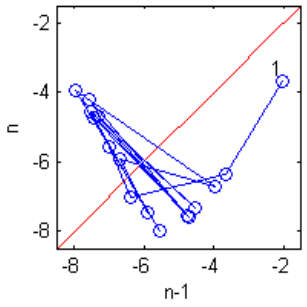
Spiral	$\dot{x}_1 = x_2$ $\dot{x}_2 = -ax_1 - bx_1^{\frac{1}{2}}$ *where a=0.2 and b=0.3*	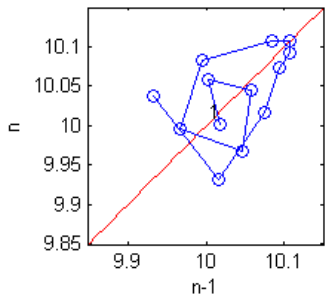	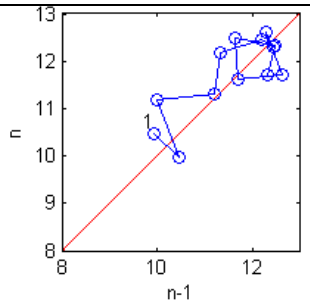
Bipolar	$\dot{x}_1 = x_3$ $\dot{x}_2 = x_3 + x_2$ $\dot{x}_3 = -\frac{b}{m}x_2 - \frac{g}{ml}\sin(x_1) - x_3$ *where g=48, m=25, b=37, and l=2*	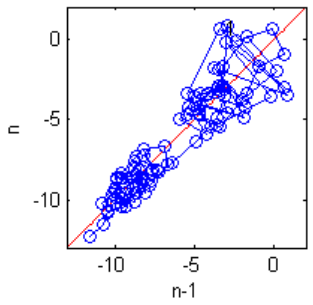	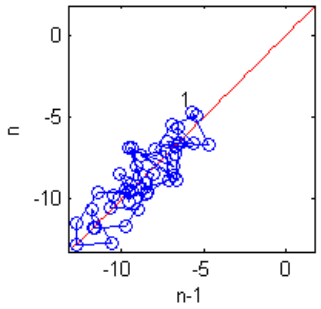
Chaotic	$\dot{x_1} = \sigma(x_2 - x_1)$ $\dot{x}_2 = \rho x_1 - x_2 - x_1 x_3$ $\dot{x}_3 = x_1 x_2 - \beta x_3$ *where* $\sigma = 10, \rho = 28,$ *and* $\beta = \frac{8}{3}$	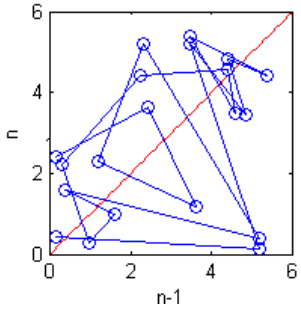	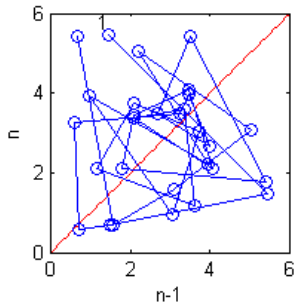

As shown in Table 3-3, the behaviour of a stable system, modelled as a mass-spring-damper system, elicits a Poincaré map with a slope of less than one that converges towards

the unity line. Comparatively, an unstable system, such as a second-order, nonlinear system, yields a slope greater than one and diverges away from the unity line. When Gaussian noise is added to the stable and unstable systems, as seen in the corresponding figures in the stochastic column of Table 3-3, the systems exhibit similar behaviour, but with greater variability as they move towards or away from the unity line. This latter behaviour may more closely resemble potential observations of stochastic EMG-based control schemes.

Other potential manifestations of dynamic systems include oscillatory, bipolar, spiral, and chaotic systems.

- Oscillatory systems intersect a Poincaré surface with a sequence of trajectory points that alternate in value. Poincaré maps of deterministic oscillatory systems, such as a Rossler Attractor, shown in Table 3-3, have little to no variation along the main differentiator axis (also called SD2, as represented in Fig. 3-5) but oscillate across the unity line, signifying instability. Stochastic oscillatory systems display more variability and a larger range across the unity line than the precise oscillations of deterministic systems, seen in the stochastic column of Table 3-3.
- Spiral systems are periodic. They are affected by the equilibrium point of the system and can converge towards, or diverge away from, the equilibrium point over time. A stochastic spiral may intersect multiple times as it moves relative to the equilibrium point and may take a longer time to reach the equilibrium point than a deterministic system (Table 3-3).
- Poincaré maps of bipolar systems, such as the damped inverted pendulum in Table 3-3, can shift from good performance to bad performance but do not alternate like

an oscillatory system. Instead, these systems fluctuate along the unity line, shifting back and forth from the top half to the bottom half of the unity line and vice versa. A person using a bipolar myoelectric co-adaptive system may experience easy and accurate control for a few repetitions of the task but suddenly find themselves losing control when reaching towards their target, or vice versa.

- An example of a chaotic system is the Lorenz attractor, modelled in Table 3-3. This system's Poincaré map neither converges to nor diverges away from the unity line but appears to move randomly when its equation is both deterministic and stochastic. However, the Poincaré plot of this chaotic system remains within a bounded radius, and the size is variable depending on the system.

Accordingly, these simulations are provided to guide the interpretation of this work's results.

3.3 Performance Metrics

Various performance metrics were recorded throughout the experiment including the time taken to reach the target, the success rate of reaching the target, the path that was taken from start to end, and the reaction time. Following each set, the subject was asked to rate their control as being either easy, reasonable, possible, or impossible, based on the perceived level of effort needed to reach the target.

3.3.1 Usability Metrics

Throughput, the standard summary performance measure obtained from a Fitts' law test, was computed during each set to measure the effects of learning, adaptation, and sparsity. Various throughput measures were used in this work, as defined in Table 2 [91]

Table 3-3: Definitions of Fitts' Law Performance Metrics Used

Metric	Definition
Throughput (TP)	Overall human performance relating the Fitts' index of difficulty to the movement time. (bits/s)
Effective Throughput (TPe)	Normalization of throughput by the effective width of the target, calculated as $4.133 * SD_x$ where SD_x is the standard deviation of the target coordinates, to increase the accuracy of the performance metric [99]. (bits/s)
Effective Throughput for all targets	The average TPe of the 20 targets per set.
Effective Throughput of target 100	The average TPe of the full-distance target on each axis per set.

An unsupervised dimensionality reduction tool, principal component analysis (PCA), was used to project the extracted features into a 2-dimensional feature space for visualization purposes. The first two PCA projections of the data from the Feedback-Enabled and testing stages from each session were plotted to identify any trends across sessions. The resulting plots demonstrated the variation in motion data across the 12 sets of target-reaching tasks, for comparison across the different protocol conditions.

User adaptation was quantified using the repeatability index (RI) and separability index (SI) metrics developed by Bunderson and Kuiken (2012) [100]. The RI index was used to measure how well the user replicated EMG patterns over the 12 sets of target-reaching tasks per session. SI was used to measure how distinguished the motions were over the 12 sets in the Feedback-Enabled and Testing stages for each session as protocol conditions changed. Both SI and RI values were normalized to allow for better

comparison across subjects and protocol changes. These indices are typically used with classification schemes and are calculated using the existing classes of motion [100], [101]. However, as a regression model was used in this work, the data collected had to be manually separated based on the amount of data that was collected per set to calculate the RI and SI values. The RI metric was reciprocated in this work to better denote value to meaning [101]. In other words, increasing repeatability and separability values over iterations signified improved pattern control and that the user was learning [101].

To support subsequent analyses, the coefficient of determination (R^2) was computed between the cursor's position on the screen and the target position for each set in the Feedback-Enabled and testing stage, as explained by Fig. 3-3. This metric, here called User-Target Position R^2, was primarily used in combination with control techniques to define user adaptation over time. The closer the R^2 value was to 1, the closer the user's cursor position matched the target position, representing strong user performance. The dynamics of the regressor were observed through the changing trends of the median of the first principal component over the 12 sets in the Feedback-Enabled and Testing stages, here called Regression Monitoring. This trend visualizes any behavioural changes in the system, such as divergence or convergence, when protocol combinations were varied. R^2 and the Regression Monitoring metric provided quantitative and qualitative means from which to evaluate user learning, machine adaptation, and concurrent adaptation of both subsystems.

3.3.2 Poincaré Standard Descriptors

Not all systems follow the example mappings seen in Table 3-3 but may instead form a radially bounded cloud of points. Such Poincaré plots can be described by their spread using the standard deviation along particular axes relative to the unity line. The label SD1 is given for the standard deviation that is perpendicular to the major axis of variation, whereas SD2 is given to the standard deviation perpendicular to the minor axis of variation (Fig. 3-5).

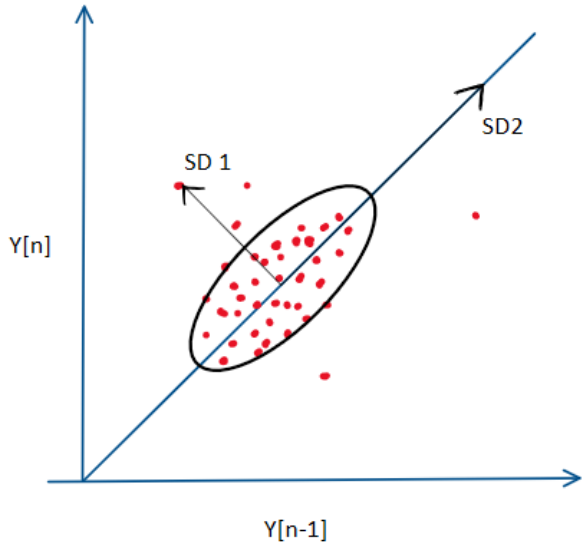

Figure 3-5: Poincaré map with both main axes labelled. SD1 and SD2 are determined by the distribution of points along the minor axis and the major axis respectively.

These two metrics represent different aspects of the system's behaviour and are mathematically defined by (6) and (7), as defined by [79], [86], [87].

$$\boldsymbol{SD1} = \frac{\sqrt{2}}{2}\boldsymbol{SD}(\boldsymbol{x_n} - \boldsymbol{x_{n+1}}) \tag{6}$$

$$\boldsymbol{SD2} = \sqrt{\boldsymbol{2SD}(\boldsymbol{x_n})^2 - \frac{\boldsymbol{1}}{\boldsymbol{2}}\boldsymbol{SD}(\boldsymbol{x_n} - \boldsymbol{x_{n+1}})^2} \tag{7}$$

SD1 represents the short-term variability of the system from one epoch to the next [79], [86], [87], [102], [103]. If SD1 is large, then the system's behaviour varies within sessions, and practically, suggests that the user is oscillating between a well-controlled repetition with good performance and a poorly controlled repetition with worse performance. If SD1 is small, then control is repeatable over time and suggests that the user is understanding the system. SD2 is the long-term variability in performance across all epochs and this progression of system performance over the span of days can be used as a measure of learning. If SD2 is large while SD1 is small, it represents a consistent learning effect without much deviation in performance.

The ratio of SD1 to SD2 is used in the Poincaré literature to represent the randomness in the variability of the system [86], [87]. This ratio characterizes the clarity, sharpness, and linearity of the scatter pattern to describe the dynamic behaviour of the time series signal without the use of a model [86], [104], [105]. A low ratio signifies higher linearity and clarity with a tighter spread along the unity line. A high ratio represents greater uncertainty in the changes in the data pattern, relating lower confidence in the co-adaptive HMI system's decisions and, therefore, inferior performance. For context, Table 3-4 and Fig. 3-6 show the ratios for the examples show in Table 3-3.

Table 3-4: SD ratio values calculated from the simulated deterministic models in Table 3-3

System Type	SD Ratio
Stable	0.143
Bipolar	0.227
Chaotic	0.731
Oscillatory	1.191
Spiral	1.399
Unstable	n/a

The relatively high SD ratios calculated from the simulated deterministic oscillatory and spiral examples in Table 3-3 signify high variability across the unity line (high SD1, seen in Fig. 3-6) without convergence to an equilibrium point. The SD ratios calculated from the deterministic stable and bipolar systems are low, representing low variation across the unity line (low SD1, Fig. 3-6) and high adaptation as time passes (high SD2, Fig. 3-6).

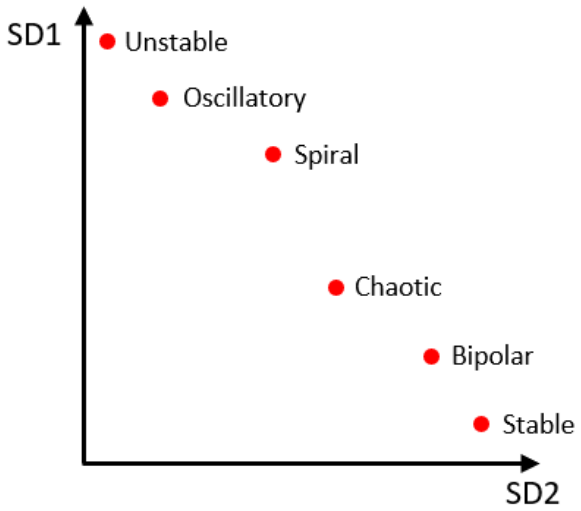

Figure 3-6: Representing the six typical Poincaré plots based on their SD1 and SD2 values

The simulated chaotic system's SD ratio showed that there was higher long-term variance than short-term variance (Fig. 3-6), but its value was not as low nor as high as the other simulated systems. The simulated unstable system was exponentially unstable, leading to an exponential difference between each time-step, a negative argument in the square root term in Eq. [3] and a complex value for the SD ratio (Table 3-4). Therefore, both practically and analytically, unstable systems exhibit unwanted dynamics. The

standard deviation metrics and their ratio are used in this work to analyse the stability of co-adaptive systems.

Now that SD values were calculated for a range of system dynamics, we can investigate how these metrics behave for co-adaptive HMIs. Ideally, a co-adaptive system would be stable with a low SD ratio. Higher SD ratios show erraticism in the system's performance and can be indicative of a disconnect between user and machine. This disconnect can arise from a delay in the system or feedback or an adaptation rate that is not sustainable by the dual-learners. If the system is not adapting and there is only one learner in the HMI, then a high ratio is expected while the user is learning how to control the system before eventually stabilizing in performance and achieving a low SD ratio. However, when the human and machine are concurrently learning without a complementary rate of adaptation, we expect a result akin to that of a chaotic system.

In this work, subjects were asked to perform the same experimental protocol 16 times per session, equating each set to a time-step and making this system periodic. The data collected from each session's Feedback-Enabled and Testing stages were analysed through five metrics. This resulted in 12 values for each metric (excepting RI and SI which had 11 values since the first day was used for comparison purposes). These values were then labelled with time-steps such that they represented the present (n) and past ($n-1$) values of the cycle. The present (n) sequence consisted of the second to the last value of each metric and the past ($n-1$) sequence consisted of the first to the penultimate value, reducing the cycle by one (11 for each metric except RI and SI which had 10). The present sequence (n) was plotted against the past sequence ($n-1$) to form the Poincaré maps.

The metrics chosen in this work focus on different aspects of the co-adaptive system. The experiment was set in a Fitts' Law environment and so a commonly used metric in myoelectric research (average effective throughput) was chosen to focus on the performance of the user and machine in a target-reaching setting. Repeatability and separability indices were chosen to measure the robustness of the pattern recognition control scheme over time. The User-Target Position R^2 was used to test the user's learning and performance through repeated iterations of the experiment. The Regression Monitoring metric was designed to measure the trends of the regressor as the level of adaptation and training data was varied in the experimental protocols. These metrics, much like the learners in a co-adaptive system, work together to provide information about how the systems behave over time. The knowledge gained by observing the behaviour of each of these metrics can be accumulated to guide further studies on the stability of chaotic co-adaptive myoelectric HMIs.

4. Results and Analysis

The objective of this work was to describe the dynamical nature of human-machine co-adaptive systems, as existing techniques do not provide this information. Poincaré maps were chosen as the tool in this work to illustrate the data for three subjects from 40 different sessions across 10 days. The data collected were analysed through three typical metrics (Fitts' Law Effective Throughput, Repeatability Index, Separability Index) and two novel metrics (User-Target Position R^2, Regression Monitoring). The time series and Poincaré maps of each of these metrics were plotted and compared. It was expected that the Poincaré mappings should provide more information about the dynamics of the system and the user-machine behaviour throughout the experiment than conventional time series. The Poincaré map provides a visual and empirical (with the aid of standard descriptors SD1, SD2, and SD ratio) evaluation of the system's dynamics over short and long periods. In this work, we compare the Poincaré plots of our case studies to that of simulated systems (Table 3-3, 3-4) to interpret co-adaptive HMI systems' dynamics.

The effects of changes in the protocol and subject's EMG control experience on learning over the 10 days were evaluated. The dynamics of the co-adaptive systems were drawn from the Poincaré maps and their associated SD values. As this visualization tool yields many plots, this section will only display comparisons between S1 (novice) and S3 (experienced), to simplify the analysis. S2 corroborated the findings of this study, and some of their results can be found in the Appendix under section 7.3. The following sections describe the observed similarities and differences between the time series and Poincaré maps for the Fitts Average TPe, Repeatability Index, and User-Target Position R^2 metrics. The results and analysis from the Separability Index and Regression

Monitoring metrics can be found in the Appendix under sections 7.1 and 7.2 respectively. The results from all five metrics agreed with the results presented in this chapter.

4.1 Fitts' Law Average Effective Throughput (TPe)

The experimental design was set in a Fitts' Law environment where the user was tested on their ability to reach a target from a starting point within a given length of time. This enabled the use of the summary TPe metric in evaluating the system performance.

4.1.1 Time Series Analysis

Fig. 4-1 shows the time series plot of the average TPe values of each set in the Feedback-Enabled and Testing stages across the 10 days. The data are organized by subject and protocol combination. A line of best fit of each subject's TPe performance over the four protocol combinations was overlaid on the subplots. From the line of best fit in Fig. 4-1, we can see that S3's performance decreased when using the sparsely-trained algorithm ($\bar{A}S, AS$), independent of algorithm adaptation. No real conclusions can be made about subject performance from the best-fit line of the TPe time series plots.

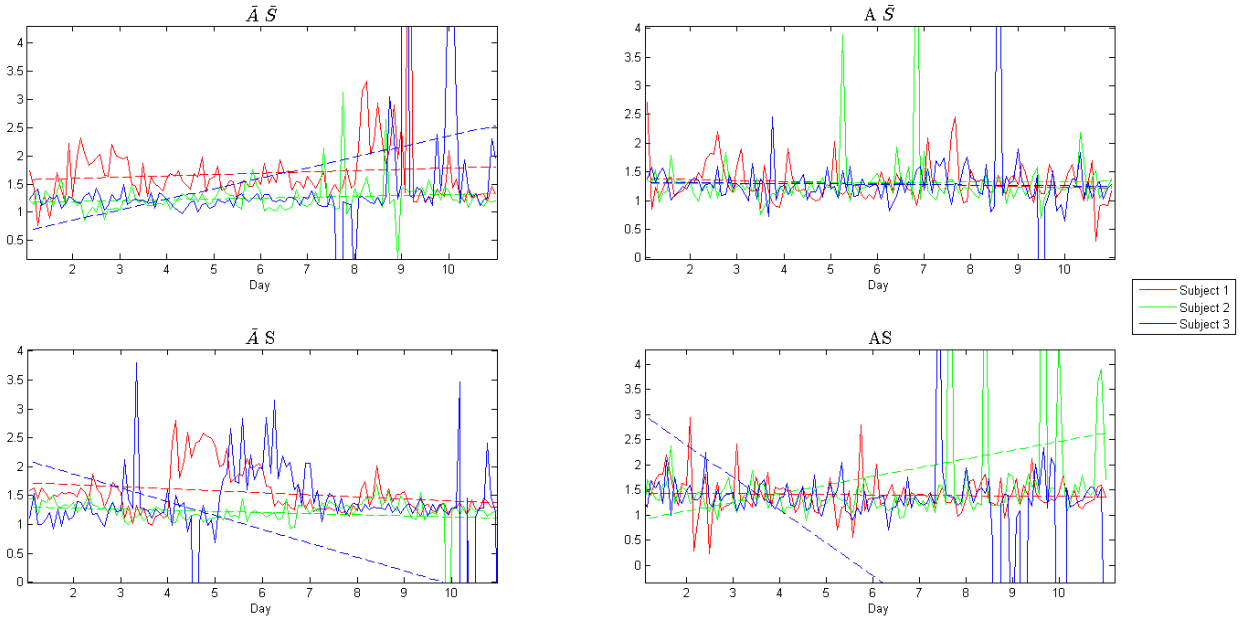

Figure 4-1: Fitts' Law average TPe for all 3 subjects over the 10 days. Dotted lines represent the line of best fit.

4.1.2 Poincaré Mapping

S1's average TPe Poincaré map is displayed in Fig. 4-2 and S3's in Fig. 4-3. S1 had the least amount of experience with EMG control and their time series did not provide substantial information, so the behaviour of their TPe through a Poincaré map was particularly informative. Higher variability across the Poincaré unity line can be seen when the adaptive protocol was used compared to the non-adaptive. Yet S1 was able to achieve higher throughput when using the non-adaptive controller, as seen by Fig. 4-2 a and c, representing a higher accuracy to speed ratio in their movements.

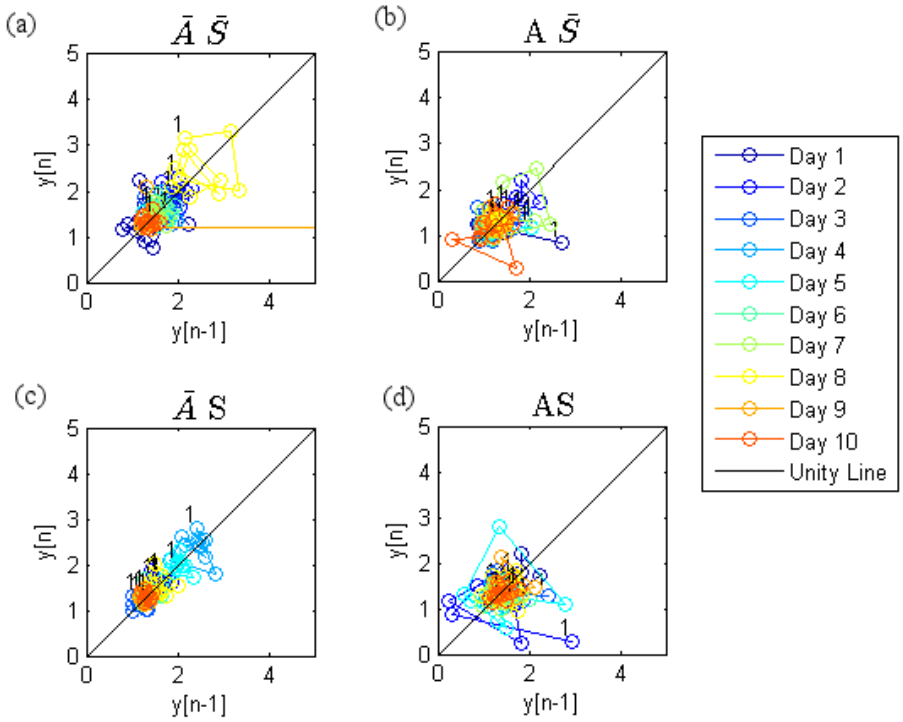

Figure 4-2: Poincaré map of Fitts' Law average TPe, S1 across the 10 days

S3's Poincaré map in Fig. 4-3 shows tightly bound TPe when training with all data (4-3a, 4-3b). One can see outlying TPe values during the subject's final days' performance in Fig. 4-3, similar to that of the time series plot in Fig. 4-1. Overlooking these outliers, we see that the subject's TPe values remained within a bounded radius which was larger during the $\bar{A}S$ protocol (4-3c) than other protocols. This enlargement is due to the increase in long-term variability seen along the unity line halfway through the subject's 10-day experiment.

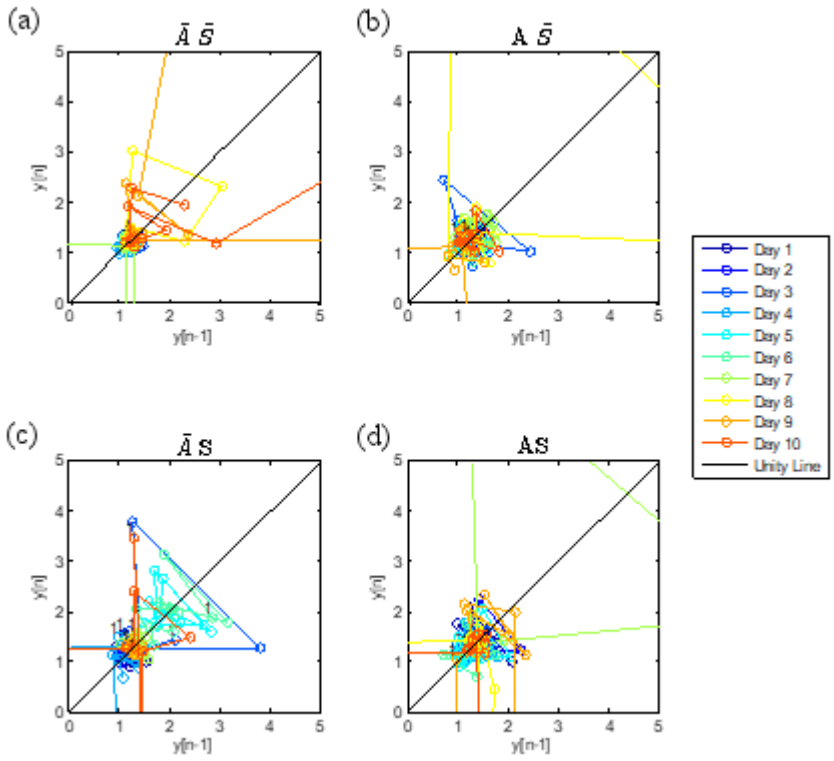

Figure 4-3: Poincaré map of Fitts' Law average TPe, S3 across the 10 days

4.1.3 Learning Analysis

It is useful to know whether a user is learning from their training sessions, so we analysed the time series TPe maps for learning effects. The Poincaré map of S1's TPe performance provides information on a learning effect over the 10 days. In Fig. 4-2d, we can see that the user initially varied widely in their effective throughput performance but was more consistent with their target-reaching motions in the final days of the experiment when controlling the adaptive, sparsely-trained (AS) system. Fig. 4-2c displays the subject's TPe performance along the unity line, rather than across it, when using the non-adapting, sparsely trained system ($\bar{A}S$). S1 ends their 10-day experiment with throughput values similar to their initial values but had higher throughput values halfway

through the experiment. The fact that there was growth along the Poincaré unity line with little deviation represents repeatable control and understanding from the user with an AS protocol.

The SD values were calculated and the ratio of SD1/SD2 for the subjects over the 10-day experiment are shown in Fig. 4-4. A ratio lower than 1 signifies that the user learned over the 10 days more than any uncertainty experienced in their control per day. The SD ratio values in Fig. 4-4 are within the range of values associated with chaotic systems, as seen in Table 3-4, and infer that the system's throughput performance is chaotic. Accordingly, the protocols involving an adaptive system, whereby the user can be confused by the changing control scheme, shows higher SD ratio values than the non-adapting protocols. S3's SD ratio while using the $\overline{AS}$ protocol is much lower than their use of the other three, representing lower randomness in their TPe performance during this protocol. S1's SD ratio is lower than their counterpart's, meaning that the novice user was able to learn more over the 10-day experiment and perform more precise target-reaching movements at each session when the algorithm was static.

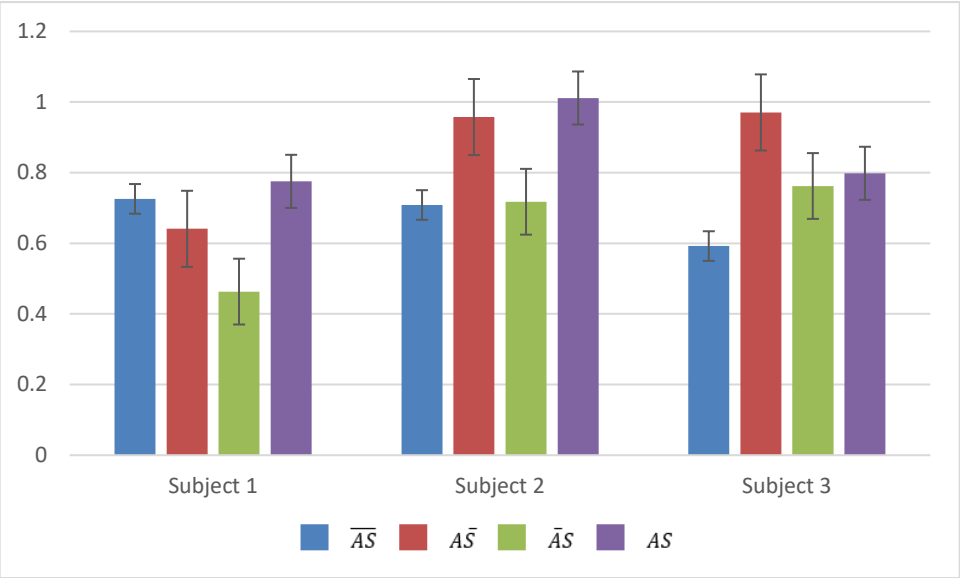

Figure 4-4: SD ratio values taken from the Fitts' Law average TPe Poincaré maps

4.1.4 Brief Summary

Comparing time series data to Poincaré maps of the case studies' Fitts' Law Average TPe metric resulted in the following findings:

- TPe performance was better for all subjects when the machine was non-adapting.
- SD1 (short-term variability) was high when S1 used the adapting protocols, and their SD ratio was accordingly high.
- S1's SD ratio was lower than that of S2 and S3, showing that there was greater long-term variability in their performance, indicative of greater learning and adaptation over the 10-day experiment.
- Poincaré maps remained within a bounded radius; SD values matched that of a chaotic system.

- These findings came from the Poincaré maps as the time series plots did not provide useful information about the co-adaptive system.

4.2 Repeatability Index (RI)

Repeatability Index can be used to monitor the robustness of a pattern recognition model to changes in EMG. The higher the RI, the better a user can reproduce EMG patterns across sets.

4.2.1 Time Series Analysis

A time series plot of the RI values taken from the Feedback-Enabled and Testing stages over the 10 days, organized by protocol combination, is displayed in Fig. 4-5. S1's time series RI plot shows various amounts of improvement in RI over the 10 days using all four combinations, as shown by the positive slope on the best-fit line. S3's decreasing trend in RI values in opposing protocols ($A\bar{S}$ in Fig. 4-5b and $\bar{A}S$ in Fig. 4-5c) was unexpected. Within the days, a decaying effect can be seen while subjects performed the adapting sessions, representing worsening repeatability as the user and machine tried to learn together. The time series of RI values show no difference in performance dependant on adaptation or training-data quantity for S1 and S3.

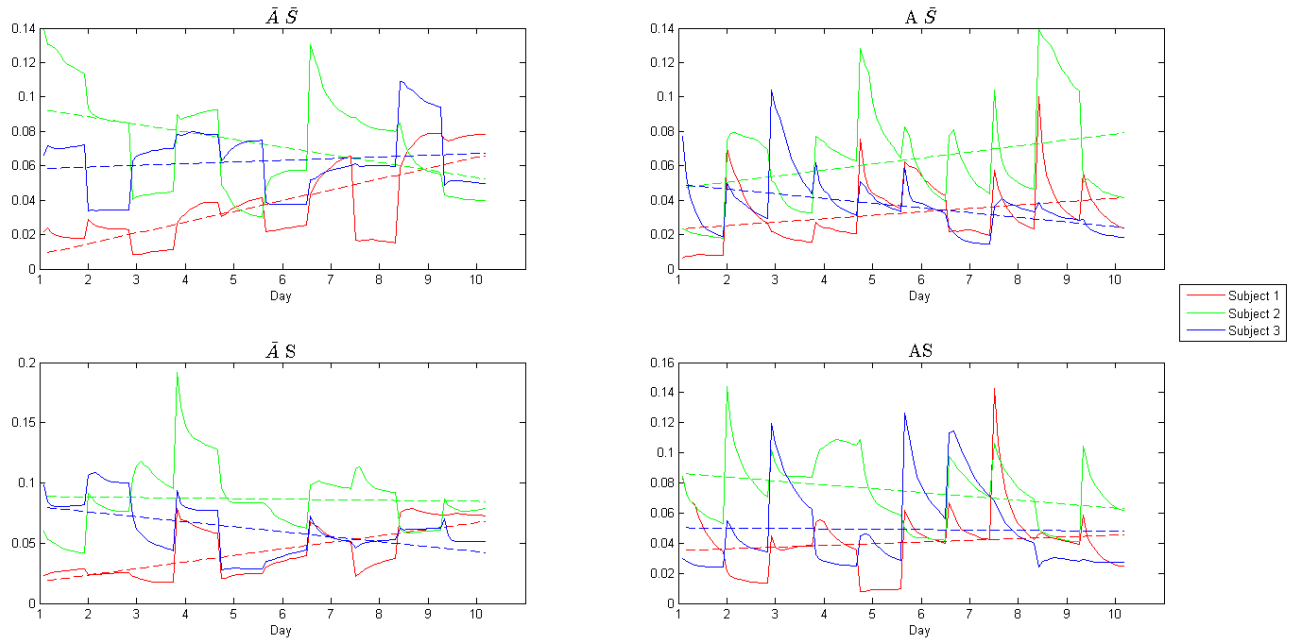

Figure 4-5: Time series plot of RI for all 3 subjects. Dotted lines represent the line of best fit.

4.2.2 Poincaré Mapping

The Poincaré maps of RI values in the Feedback-Enabled and Testing stages were plotted to observe the trend over the 10 days and to compare the information to that provided by the time series plot in Fig. 4-5. A steady improvement in S1's repeatability during the use of the $\overline{AS}$ protocol can be noted in Fig. 4-6a over the 10 days. There is very little variability across the unity line, suggesting consistent control, and each day's repeatability values are better than the previous (excepting Day 8), suggesting an improved understanding of control. S1's improved repeatability is also visible in Fig. 4-6c, albeit to a lesser extent, during their use of the non-adapting, sparsely trained protocol ($\bar{A}S$). However, their control changes when the system adapts. Fig. 4-6b and 4-6d show that the user begins each day's session further from the unity line but then converges towards it, representing unsure EMG control at the beginning of the sets but stabilizing

before the session is over. When the user operates with the adapting algorithm, their RI values at the end of the 10 sessions are not as high as when the system is non-adapting. Additionally, S1's ability to be repeatable at the end of the 10 days is similar to their ability at the beginning of the experiment, following a bipolar trend between low and high performance. This movement seemingly negates any learning improvement made throughout the 10 days and requires further research to know whether this is common behaviour in co-adaptive HMIs.

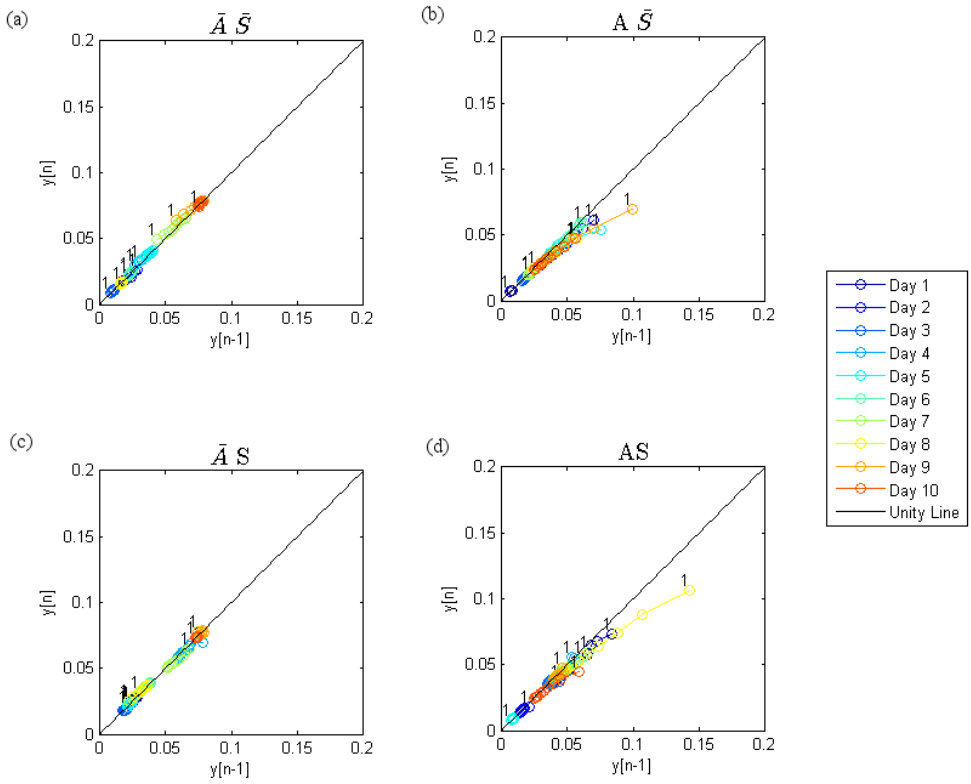

Figure 4-6: Poincaré plot of S1's RI values across the 10 days

S3's RI Poincaré map (Fig. 4-7) agrees with the time series plot (Fig. 4-5) in that the user's RI values decreased as the number of sessions increased when the user performed the $A\bar{S}$ (Fig. 4-7b) and $\bar{A}S$ (Fig. 4-7c) protocol combinations. However, with

the Poincaré map in Fig. 4-7, we can more specifically describe the user's decrease in repeatability. For example, in Fig. 4-7c, when the algorithm is non-adapting, the user's daily RI values are distinct from each other, whereas when the user used the adapting algorithm (Fig. 4-7b), the RI values are muddled and the ranges are widespread and overlapping. This phenomenon, also seen when comparing Fig. 4-7a and 4-7d, implies that S3 adapts more quickly as the algorithm adapts than when it is static. While the final values for the user's RI are lower when the algorithm is adapting than static, the knowledge that the user is exploring and learning is constructive to the design of future co-adaptive EMG controlled tasks, as this knowledge can be used to control the co-adaptive system more advantageously.

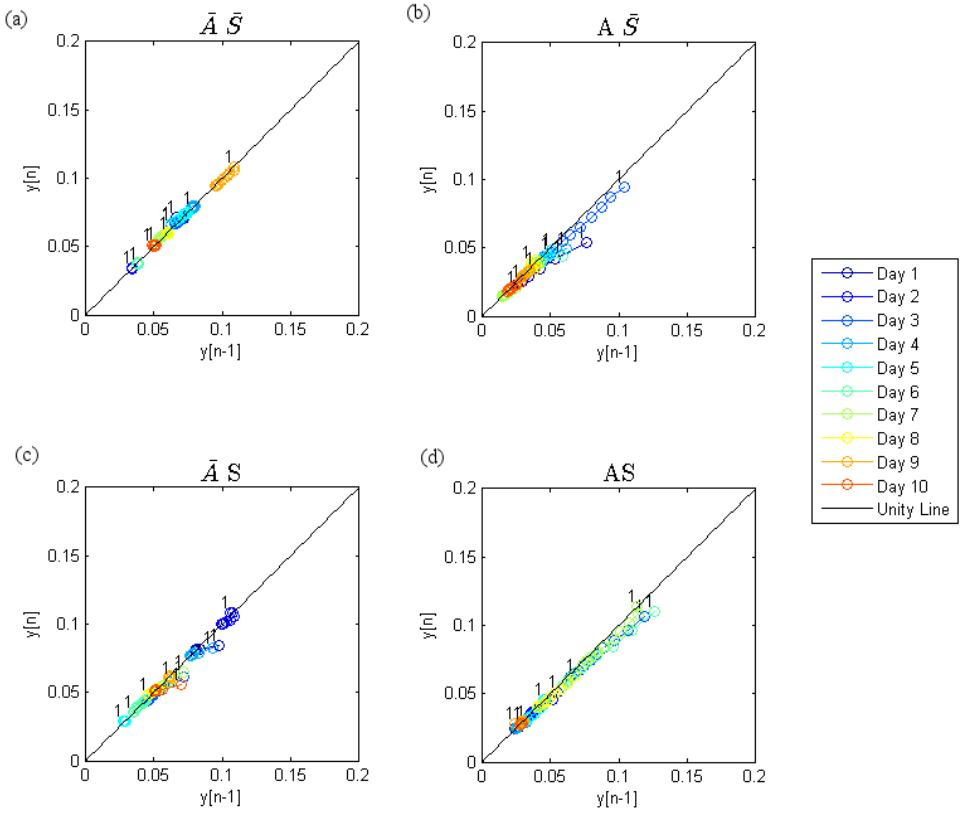

Figure 4-7: Poincaré map of S3's RI values across the 10 days

4.2.3 Learning Analysis

Through the Poincaré plots, we can contrast each user's RI values over the 10 days, and visually ascertain possible learning effects. S1, the least experienced with EMG control, improves more markedly than the other subjects, particularly when there is no algorithm adaptation. On the other hand, while S3 does not deliver higher RI values for the experiment, their wide range in RI values along the unity line suggest that learning is occurring, but the user is uncertain of their control and they are not improving. S3's RI values "bounce" along the unity line, fluctuating between high and low values over the 10 days. This behaviour seems random but resembles the behaviour of a typical bipolar Poincaré system, as demonstrated in Table 3-3, exemplifying the chaotic nature of a co-adaptive EMG system.

The analysis of the user's data through the RI metric can be accomplished visually or quantitively from the Poincaré map. All three subjects' individual days displayed behaviour comparable to that of a stable Poincaré map, shown in Table 3-3 wherein the RI values converged towards the unity line. In cases where there was algorithm adaptation, the user's initial RI values were further away from the unity line. As such, convergence only occurred after most of the sets in the Feedback-Enabled and Testing stages were completed (such as in Fig. 4-6d and Fig. 4-7b, 4-7d), rather than an immediate convergence when there was no adaptation in the algorithm, as seen in Fig. 4-6c and 4-7a. The number of sets required for the user to converge to a stable point depended on the algorithm adaptation.

From the SD ratios calculated (Fig. 4-8), we observe a difference based on algorithm adaptation: low ratios with non-adapting algorithms and high ratios with

adapting algorithms. Without the added uncertainty of an adapting algorithm, users were able to control their contractions throughout the experiment and improve on their repeatability as days increased. Note that the values of the RI SD ratios are much lower than those of the Fitts' Law average TPe in Fig. 4-4, suggesting very low variance and sufficient improvement when measuring the repeatability of the users' actions rather than their throughput. These low values can be compared to the low SD ratio value calculated from the typical, stable Poincaré plot in our simulated equations in Table 3-4.

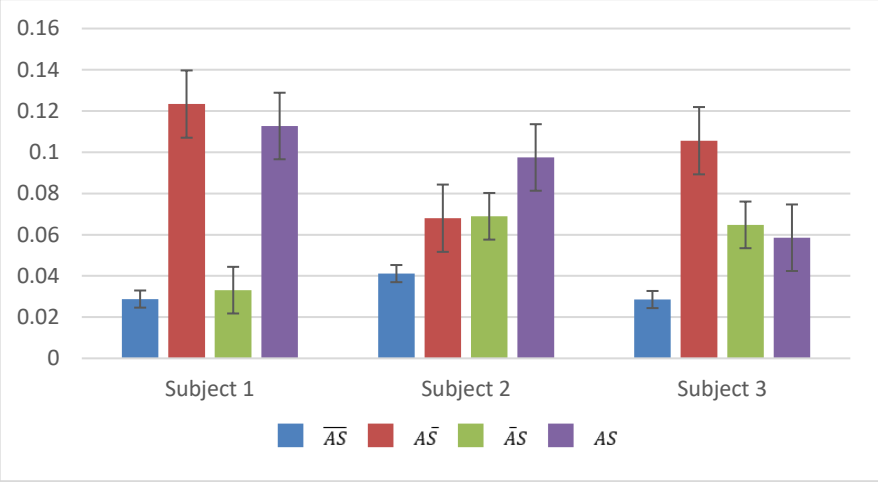

Figure 4-8: SD ratio calculated from the Poincaré map of the RI values of three subjects across the 10 days

4.2.4 Brief Summary

The RI values plotted and compared through time series and Poincaré maps resulted in the following findings:

- Time series plots show general improvement among subjects.
- Non-adaptive protocols showed better repeatability.

- Poincaré maps also show user improvement but explain the co-adaptive system behaviour during the improvement. Particularly, a bipolar dynamic was observed across S3's 10-day data.
- Convergence towards the unity line within a day's session was observed through the Poincaré map and SD values.

4.3 User-Target Position R^2

The coefficient of determination (R^2) between the user's cursor position and the target position was calculated for each of the 20 targets in a set, then averaged for each set in the Feedback-Enabled and Testing stages. A value closer to 1 means that the user can precisely control their EMG contractions to position the cursor on the target. The next sections describe the R^2 results as time series plots and Poincaré maps, then compare the observed learning effects for each.

4.3.1 Time Series Analysis

The time series plots of the user-target position R^2 are shown in Fig. 4-9 and Fig. 4-10 for the regression models trained for DOF 1 and DOF 2, respectively. Except for S1's low performance at the start of the experiment and on Day 8, we notice that the three subjects were able to maintain higher R^2 values in both DOF 1 and DOF 2 when using the non-adapting algorithm. When the subjects used the adaptive protocols, the correlation between their cursor position and target position varied widely, they were unable to respond appropriately to the adaptations in both DOF 1 (Fig. 4-9) and DOF 2 (Fig. 4-10). The line of best fit for these protocols denotes a positive change in R^2 over the 10 days

but, even with the improvement, the end values of R^2 were not as great as when there was no algorithm adaptation.

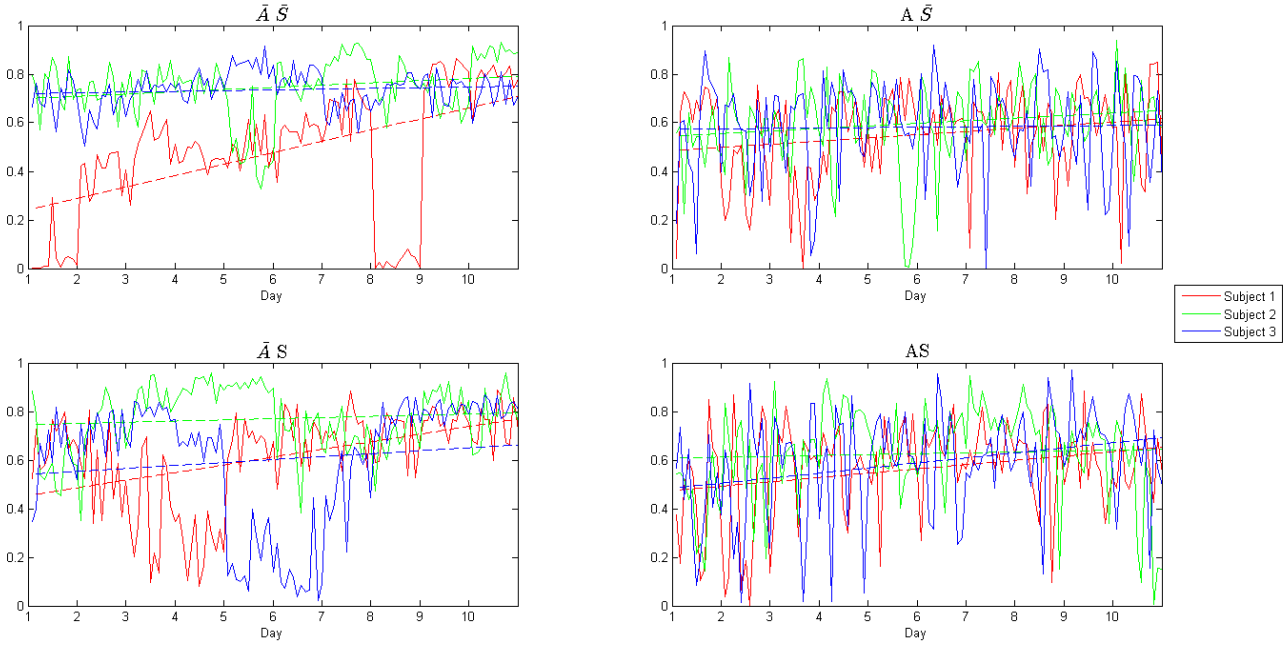

Figure 4-9: Time series maps of user-target position R^2 of DOF 1 over the 10 days. Dotted lines represent the line of best fit.

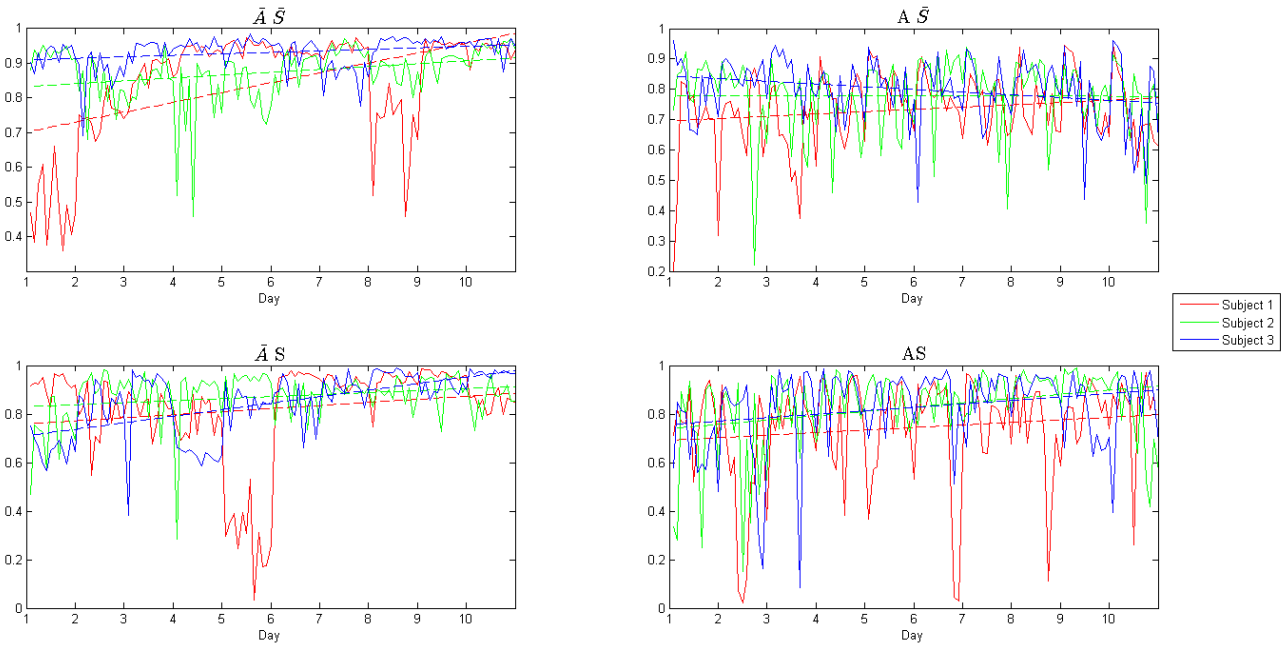

Figure 4-10: Time series plot of user-target position R^2 of DOF 2 over the 10 days. Dotted lines represent the line of best fit.

4.3.2 Poincaré Mapping

The Poincaré map of the user-target position R^2 was plotted to observe any chaotic behaviour in the performance throughout the various protocol versions. Fig. 4-11 shows the Poincaré plot of the user-target correlations for S1 and S3 when they performed the $\overline{AS}$ protocol. Fig. 4-11a and 4-11c show that S1's performance increased as the days went on. Except for Day 8, S1 was able to improve while using the non-adapting, non-sparsely trained system ($\overline{AS}$) to better relate the cursor to the target. On the other hand, Fig. 4-11b and 4-11d show that S3, the most experienced subject tested, did not undergo such a drastic change in performance over the 10 days. S3 was able to maintain strong performance with little changes over the 10 days.

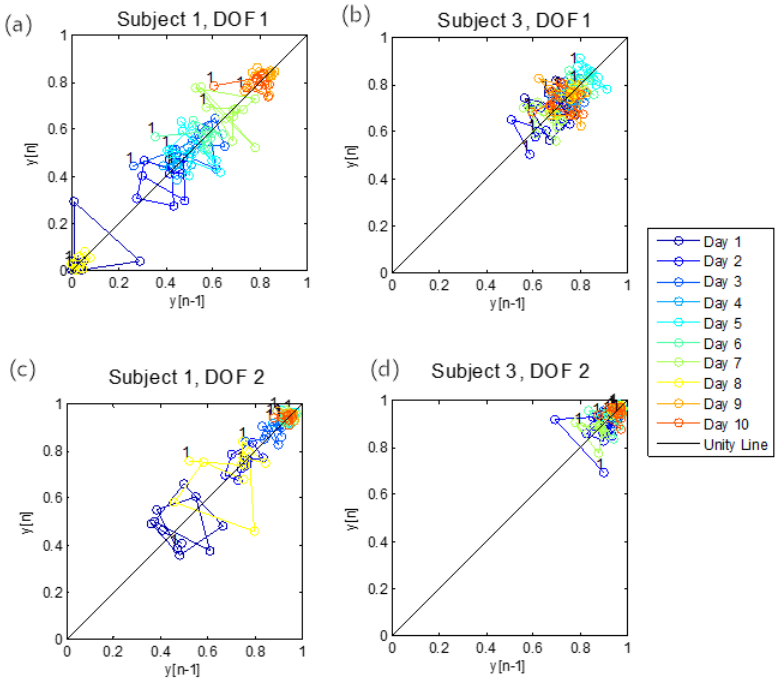

Figure 4-11: Poincaré plot comparing S1 and S3 user-target position R2 for ($\overline{AS}$) sessions

Conversely, when the adapting algorithm was used ($A\bar{S}$), similar variations were found in user-target position R^2 values between the novice (Fig. 4-12a) and the experienced subject (Fig. 4-12b). In Fig. 4-7d, S3's performance at the end of the 10-day experiment is lower than their performance at the start of the experiment. Additionally, S3's Poincaré map is more variable across the unity line at the end of the experiment, signifying uncertainty in their actions after days' worth of training. S1 begins their 10-day experiment with similar uncertainty, but their variability lessens as time increases. We can observe an improvement in R^2 values in the subjects' DOF 2 performance (Fig. 4-12c and 4-12d), but there is as much uncertainty in both subjects, as seen by the widely varying R^2 values, regardless of skill level or length of time acquainted with the experiment.

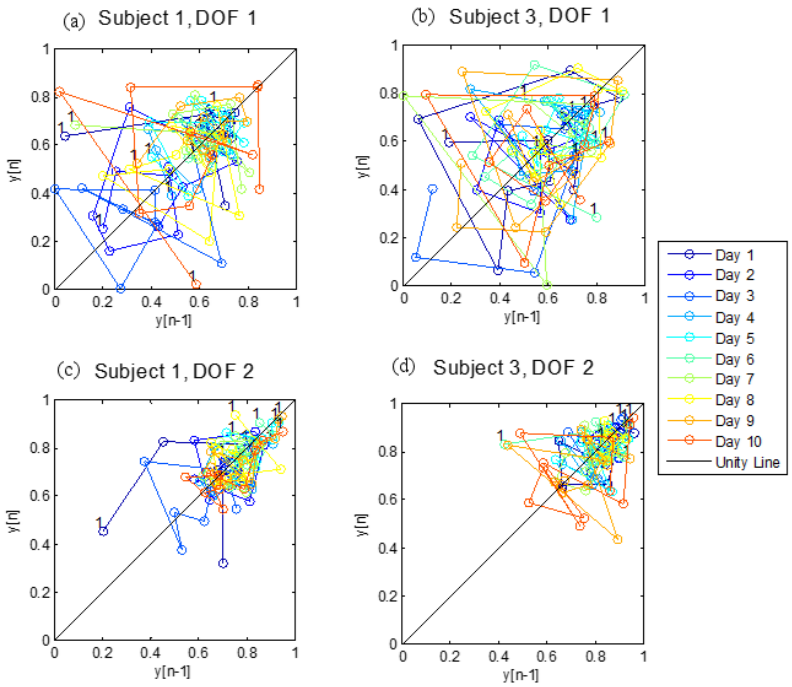

Figure 4-12: Comparing S1 and 3's user-target R^2 performance using the $A\bar{S}$ protocol

Through the Poincaré map of the user-target position R^2 metric, we can also observe changes in the subjects when the algorithm trained on a sparse dataset or a full dataset. Recall that the user was never aware when the algorithm changed its training method, as they performed the same actions to reach the same target distances throughout the experiment. In Fig. 4-13, the R^2 values for S1 and S3 are shown when using the non-adapting, sparsely trained algorithm ($\bar{A}S$). We observe that both users performed better at the end of the 10-day experiment in both DOF control. We also note that S3's R^2 values are more compact around the unity line than S1's horizontally-varying values, representing more precise control in S3's actions. S3's DOF 1 actions are particularly interesting, as they begin the 10-day experiment with reasonably good R^2 values (between 0.6 and 0.8), then perform quite badly halfway throughout the experiment (range of 0.1 to 0.6), but return to their original performance level in the final days of the experiment. This

behaviour resembles that of the bipolar Poincaré map in Table 3-3, shifting between regions of good performance and bad performance along the unity line. Knowing whether a co-adaptive system behaves in this way can lead to future studies that consider this period of poor performance to design more robust systems.

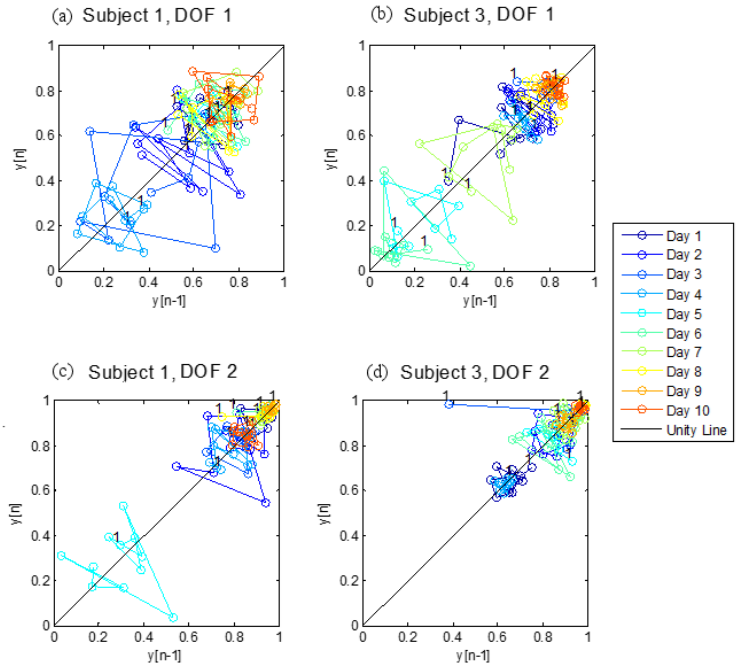

Figure 4-13: Poincaré map of S1 and S3's user-target R^2 while performing the $\overline{AS}$ protocol

4.3.3 Learning Analysis

The time series plots of the user-target position R^2 show S1's learning progress as they performed the non-adaptive, non-sparsely trained dataset ($\overline{AS}$) over the 10 days (Fig. 4-9a, Fig. 4-10a). The sharp improvement in their R^2 values over the 10 days suggests that they were able to learn from the feedback of their actions. S1 was still able to learn when the system was adapting, as seen by the time series plot Fig. 4-9d, but the amount of

improvement during the 10 days was lower than when they used the non-adapting protocols.

The Poincaré map of the R^2 values highlights the presence of a learning effect by comparing the difference in performance between S1 and S3 when the algorithm was adapting and non-adapting. Specifically, the novice user improved when they adapted and learned from the static machine, but the user who already had experience showed less improvement. When the algorithm adapted with the user, no matter the experience level, the users struggled to adapt correspondingly, leading to poor performance. This observation stems from Fig. 4-11, which compares the subjects' performances during the $\overline{AS}$ sessions, and Fig. 4-12, which compares the subjects' performance during the $A\bar{S}$ protocol sessions. Therefore, in such an aggressively adapting HMI, even a high degree of experience with EMG control may not be sufficient to overcome the degree of learning required by the subject.

The SD ratio values shown in Fig. 4-14 emphasize the effect that an adapting algorithm has on the variability of a co-adaptive system. Low SD ratios were calculated from sessions using a static algorithm whereas high SD ratios were calculated from sessions using adapting algorithms. The higher SD ratio values suggest high disorder during the sessions or little learning throughout the 10 days.

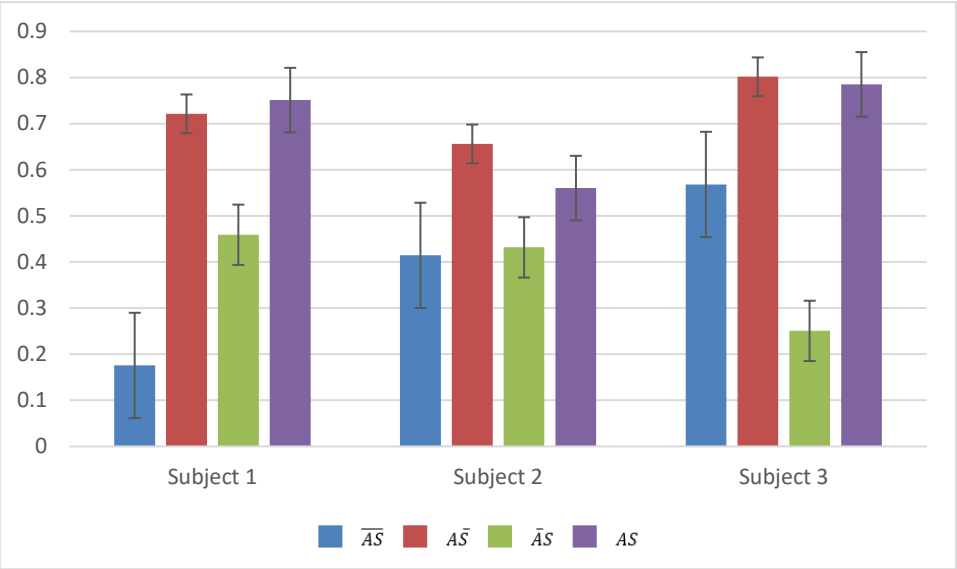

Figure 4-14: SD ratio values calculated from the user-target R^2 for DOF 1 Poincaré map across the 10 days

Interestingly, Fig. 4-14 does not confirm the effect, or lack thereof, of myoelectric control experience on the behaviour of a co-adaptive system, as seen by the Poincaré maps in Fig. 4-11 to 4-13. A closer look at the SD2 values was therefore taken, as seen in Fig. 4-15. The learning effect was much stronger in S1 than S3 when using the non-adaptive, non-sparsely trained system ($\overline{AS}$) but was similar when the experiment used the adaptive, non-sparsely trained system ($A\bar{S}$). The presence of this learning effect in the $\overline{AS}$ SD2 values, combined with the lack of learning effect in the $\overline{AS}$ SD ratios (Fig. 4-13), tells us that there was high uncertainty in the novice user's actions as compared to the amount of learning they underwent over the 10 days. Conversely, the experienced user did not portray this same variability. This distinction between user experience, algorithm adaptation, and variability in daily use is notable and should be considered when training co-adaptive systems.

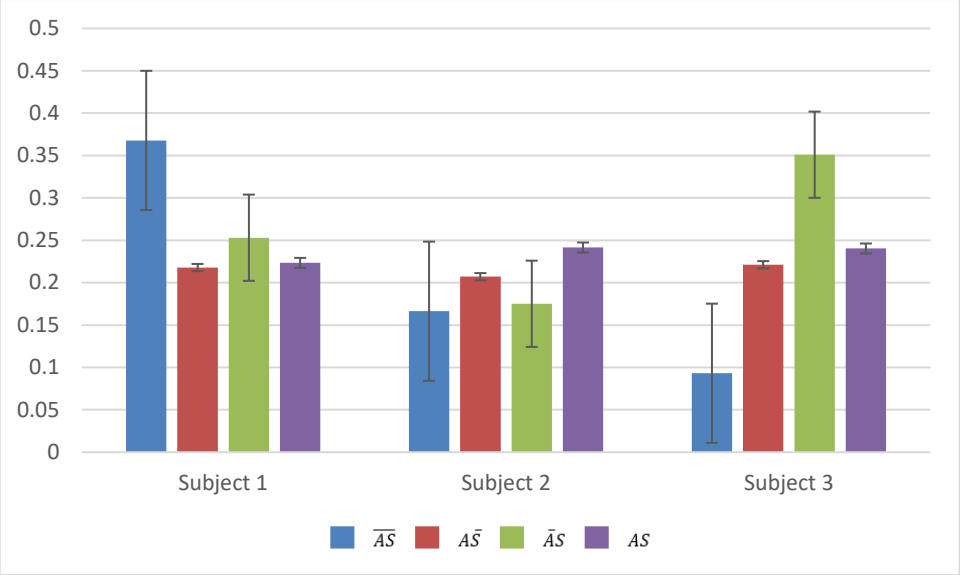

Figure 4-15: SD2 values calculated from the Poincaré maps of user-target position R^2 across the 10 days

4.3.4 Brief Summary

Comparing the time series plot to the Poincaré plot of the User-Target Position R^2 resulted in the following findings:

- Higher performance values were achieved during non-adapting protocols than adapting protocols, as evidenced by both the time series plots and Poincaré plots.
- The Poincaré plots of this metric, in particular, showed that user experience has an effect on learning, with lower experience leading to greater adaptation.
- The higher short-term variability (SD1) results suggest uncertainty between user and machine when both inexperience (S1) and the use of adapting protocols (regardless of experience) were a factor in the co-adaptive system. The novice user was able to decrease this uncertainty with the non-adapting protocol, but little change was seen for either user when using the adapting protocol.

4.4 Summary of Results

All metrics tested in this work showed how Poincaré maps and their descriptor values can provide additional information than time series plots alone. The additional knowledge pertained to the dynamics of the co-adaptive system during and across 10 days of training and testing. Stable, bipolar, and chaotic dynamics were observed through the Poincaré plots both visually and quantitatively through the SD values calculated. There was higher short-term variability, representing uncertainty, in the system when users used the adapting protocols. In the RI and R^2 metric, the long-term variability was high when a novice user performed with the non-adapting algorithm, signifying user adaptation over time. Comparatively, the level of previous myoelectric experience did not influence the amount of adaptation and performance precision when the fully adapting algorithm was used, as observed using the User-Target Position R^2 metric. These results demonstrate the power of the Poincaré maps in interpreting the behaviour of co-adaptive systems and extracting insights related experience, user learning, and machine adaptation.

5. Discussion

This work leveraged a control technique to explore the dynamics of co-adaptive myoelectric control systems and how they change over time. Experimental parameters were varied to simulate and evaluate factors that affect HMI performance in the field and the effect that machine adaptation has on the user. By using Poincaré maps, the effects of user learning over 10 days and the dynamics produced by randomness of variation in the control system were identified. The learning effects depend on mutual adaptation between the user and machine states, causing the relatively high order and nonlinearity of the system. The observed variations in performance show that the co-adaptive system may shift between stable and unstable equilibrium points. This knowledge suggests that co-adaptive myoelectric control systems are indeed chaotic.

Learning, especially during the training of a myoelectric device, is important because skills learned during training can be transferred to regular use [106] and proper training leads to higher acceptance rates of myoelectric prostheses [107]. In this work, Poincaré maps described learning effects over several days by summarizing relatively large amounts of data into clear graphs, and enabling the quantification of resultant standard deviation values. A strong learning effect was noted over the 10 days when the algorithm was non-adapting and the full dataset was used for training. This suggests that subjects, especially novice users, were able to adapt to the static, well-informed model over time. When the machine adapted concurrently with the user, however, subjects lost the ability to learn and improve over time. In this case, regardless of level of experience, subjects remained uncertain in their control during both AS and $A\overline{S}$ sessions. This is a noteworthy observation since S3 used their experience with EMG control to demonstrate repeatable,

separable, and precise control when the system followed a typical model ($\overline{AS}$). The use of Poincaré plots to visualize and assess the chosen metrics effectively highlighted the impact of the adapting system on the users' understanding of the system and of their learning on the performance of the system.

Time series-based visualizations can expose if motor performance becomes more consistent with time [67], but do not directly relate to the internal dynamics of the human-machine system or explain the reasons behind it [1]. As an example, the RI time series in Fig. 4-5 indicated consistent user improvement, and while the corresponding Poincaré maps in Fig. 4-6 and 4-7 also related improved performance, they also exposed the uncertainty introduced when the system adapted, and the bipolar dynamics of the co-adaptive system over the 10 days. The high number of sets required to converge and stabilize the user's RI values when the algorithm was adapting suggests that the user began with a poor internal model but improved as the number of sets increased and the user gained a better understanding of the HMI. The bipolar dynamics observed over the duration of the experiment suggest an interesting interaction between the user and machine and warrants further investigation into the prevalence, frequency, and duration of this behaviour. The internal dynamics of these co-adaptive systems clearly influence their practical usage and an ability to better elucidate and understand these dynamics may hold the key to stabilizing the control of co-adaptive systems.

The novel application of Poincaré maps in myoelectric studies is a simple and easy way to investigate the trends and effects of co-adaptation. Learning effects, particularly in relation to machine learning ($A/\bar{A}$) and changes in the training environment ($S/\bar{S}$), were observable when using the Poincaré maps. A clear improvement of performance was

visible in users when there was no adaptation, but confusion and a loss of learning were apparent when the model was adaptive. Additional information about the effect of adaptation on performance was noted from the Poincaré maps, such as the stable and bipolar dynamics observed in the RI values dependant on protocol variations, the spiral dynamics of the SI values (Appendix, 7.1), and the radially-bounded randomness of the Regression Monitoring Metric (Appendix, 7.2). These observations advocate that co-adaptive systems are stochastic and chaotic and the stability of the system depends on user states relative to the system's equilibrium points. Analysing the chaos in these systems using Poincaré maps provides a new appreciation of these behaviours and may inform why pattern recognition-based myoelectric control systems sometimes seem to simply stop working well.

The development of robust myoelectric systems that can maintain good performance over time has been the focus of research for years. This work supports that this may be related to chaotic nature of these systems and thus a control perspective is warranted. Ideally, the dual-learner system should be modelled with differential equations for use with control techniques to create stable systems, such as those performed by Zhang and Chase [74], [108]. Even with a model, metrics that analyse the system's stability are required, which was the focus of this work. Using Poincaré maps, we were able to identify that fully adapting algorithms and/or non-adapting algorithms with insufficient training may result in unstable systems. Applying the same controls technique presented in this work and expanding it to other metrics, such as classification accuracy, may provide valuable insight into the dynamics of dual-learner systems.

Moving forward in this field, the stochastic, chaotic elements in co-adaptive HMIs should be analysed and taken into consideration when designing myoelectric control systems. This work showed how Poincaré maps, our chosen method of analysing chaos, can be used to visualize user learning in the presence or absence of algorithm adaptation. With this tool, we discerned that the system is less stable if the human and machine are trained on different datasets (S vs $\bar{S}$), suggesting the merit in maintaining constant or slowly changing parameters in the training stage of myoelectric prostheses. Nonlinear stochastic systems, particularly chaotic co-adaptive myoelectric control schemes, contain important information but require appropriate techniques to properly appreciate their dynamics as the human and machine adapt together.

The Curious Case of Day 8

Chapter 4 alluded that the results from S1's Day 8 $\overline{AS}$ did not follow the observed trends of the other collected datasets. The definitive reason behind this is unknown, but it must be noted that the use of Poincaré maps highlighted that day's performance as abnormal. The Poincaré map's trend and meaning over the 10 days are so well-defined that it is easily noticeable when an oddity is present, such as in Fig. 4-2, 4-6, 4-10, and 4-11. Such outlier detection could be useful to ensure quality control in future research and clinical applications.

5.2 Contributions

The key contributions from this work include:

1. The exploration of the dynamics, and the identification of chaotic behaviours, in a co-adaptive HMI.
2. The introduction of Poincaré maps as a viable and informative tool for summarizing and analysing system dynamics and user behaviours over time.
3. The evaluation of user learning over a 10-day (40 session) study and the impact of adaption, user experience, and training sparsity on internal model formation.

5.3 Limitations and Future Work

This work achieved its objective of analysing HMI co-adaptive system dynamics using Poincaré maps, but a few limitations should be noted. There was a low number of subjects in this experiment, due in part to the restrictions associated with the COVID-19 pandemic. The subjects varied in experience with myoelectric control and age, but all subjects were female with similar backgrounds, so the possible user population was not accurately represented. Additionally, one of the three subjects was the author of this work and knew it's aims and experimental protocols. Unconscious biases while experimenting were therefore a possibility. This work, therefore, refrains from making large generalizations about the results, focusing instead on the importance of considering the dynamics of co-adaptive human-machine interfaces from a control perspective.

Another limitation in this work stems from the use of ‘all or none’ adaptation. Adaptation and its effects on system behaviour were analysed, but only the no adaptation or full adaptation cases were explored in the experiments. In adaptive algorithm research and practical applications, full adaptation is rarely used, so future works should evaluate

various levels of adaptation to better explain existing models. Poincaré maps could then be used to describe the dynamics when the adaptation rate is between 0% and 100% and identify the best rates. As this work set out to explore the presence of chaos in co-adaptive systems, it was beneficial to begin with the extremes to emphasize trends. Nevertheless, we hope that this work can lead to finding an adaptive rate that allows humans and machines to learn concurrently in a stable manner.

This work can be used to inform future myoelectric control experiments, to analyse existing models, and to design better ones using control techniques. For example, inertial measurement unit (IMU) sensors can be included in the co-adaptive system to observe the change in the user's wrist or arm actions as they control a cursor on the screen. Poincaré maps could then be used to compare the user's cursor data and their IMU data and analyse whether performance stability is different as a result of changing internal models. Research that compares the performance of different classifiers, which sometimes plateau over time [109], may benefit from this work to further understand the reason behind this convergence in the system.

6. Conclusion

The goal of this study was to describe the chaotic behaviour of co-adaptive myoelectric human-machine interfaces. This was achieved using Poincaré maps, a control theory-based technique used to visualize the dynamics of the system's performance. A 10-day experiment was designed and implemented to assess user performance while using a co-adaptive myoelectric system. Two variables in the machine algorithm- machine adaptation and amount of training data- were varied to elucidate the chaotic behaviour observed in the literature. Five performance metrics were then plotted as time series and Poincaré maps to enable analysis of the dynamics of over the 10 days. Chaotic behaviours, such as seemingly random variations in system performance, were observable using the proposed Poincaré maps. A learning element was apparent within certain experimental parameters but not with others, indicating the effect that improperly designed co-adaptation may have on the development of internal models and user performance with their myoelectric device. Elucidating the chaotic elements in the dynamics of co-adaptive human-machine myoelectric systems leads to a stronger understanding of these systems and the potential development of more robust designs.

Bibliography

[1] E. Biddiss and T. Chau, “Upper limb prosthesis use and abandonment: A survey of the last 25 years,” *Prosthet. Orthot. Int.*, vol. 31, no. 3, pp. 236–257, 2007, doi: 10.1080/03093640600994581.

[2] S. Mick, D. Cattaert, F. Paclet, P. Y. Oudeyer, and A. De Rugy, “Performance and usability of various robotic arm control modes from human force signals,” *Front. Neurorobot.*, vol. 11, no. OCT, pp. 1–16, 2017, doi: 10.3389/fnbot.2017.00055.

[3] E. Scheme and K. Englehart, “Electromyogram pattern recognition for control of powered upper-limb prostheses: State of the art and challenges for clinical use,” *J. Rehabil. Res. Dev.*, vol. 48, no. 6, pp. 643–660, 2011, doi: 10.1682/JRRD.2010.09.0177.

[4] E. Campbell, A. Phinyomark, and E. Scheme, “Current Trends and Confounding Factors in Myoelectric Control : Limb Position and Contraction Intensity,” *Sensors*, pp. 1–44, 2020, doi: 10.3390/s20061613.

[5] L. Hargrove, K. Englehart, and B. Hudgins, “A training strategy to reduce classification degradation due to electrode displacements in pattern recognition based myoelectric control,” *Biomed. Signal Process. Control*, vol. 3, no. 2, pp. 175–180, 2008, doi: 10.1016/j.bspc.2007.11.005.

[6] B. Hudgins, P. Parker, and R. N. Scott, “A New Strategy for Multifunction Myoelectric Control,” *IEEE Trans. Biomed. Eng.*, vol. 40, no. 1, pp. 82–94, 1993, doi: 10.1109/10.204774.

[7] J. Liu, X. Sheng, D. Zhang, N. Jiang, and X. Zhu, “Towards Zero Retraining for

Myoelectric Control Based on Common Model Component Analysis," *IEEE Trans. Neural Syst. Rehabil. Eng.*, vol. 24, no. 4, pp. 444–454, 2016, doi: 10.1109/TNSRE.2015.2420654.

[8] R. Clingman and P. Pidcoe, "A novel myoelectric training device for upper limb prostheses," *IEEE Trans Neural Syst Rehabil Eng*, vol. 22, no. 4, pp. 879–85, 2014, doi: 10.1109/TNSRE.2014.2315046.

[9] M. A. Powell and N. V. Thakor, "A training strategy for learning pattern recognition control for myoelectric prostheses," *J. Prosthetics Orthot.*, vol. 25, no. 1, pp. 30–41, 2013, doi: 10.1097/JPO.0b013e31827af7c1.

[10] J. W. Sensinger, B. A. Lock, and T. A. Kuiken, "Adaptive pattern recognition of myoelectric signals: Exploration of conceptual framework and practical algorithms," *IEEE Trans. Neural Syst. Rehabil. Eng.*, vol. 17, no. 3, pp. 270–278, 2009, doi: 10.1109/TNSRE.2009.2023282.

[11] C. Vidaurre, M. Kawanabe, P. Von Bünau, B. Blankertz, and K. R. Müller, "Toward unsupervised adaptation of LDA for brain-computer interfaces," *IEEE Trans. Biomed. Eng.*, vol. 58, no. 3 PART 1, pp. 587–597, 2011, doi: 10.1109/TBME.2010.2093133.

[12] A. Krasoulis, S. Vijayakumar, and K. Nazarpour, "Effect of User Practice on Prosthetic Finger Control With an Intuitive Myoelectric Decoder," *Front. Neurosci.*, vol. 13, no. September, pp. 1–16, 2019, doi: 10.3389/fnins.2019.00891.

[13] J. Hahne, M. Markovic, and D. Farina, "User adaptation in Myoelectric Man-Machine Interfaces," *Sci. Rep.*, vol. 7, no. 1, p. 4437, 2017, doi: 10.1038/s41598-017-04255-x.

[14] J. Hahne, S. Dahne, H.-J. Hwang, K.-R. Muller, and L. Parra, "Concurrent Adaptation of Human and Machine Improves Simultaneous and Proportional Myoelelectric Control," *IEEE Trans. Neural Syst. Rehabil. Eng.*, vol. 23, no. 4, pp. 618–627, 2015, Accessed: Dec. 08, 2017. [Online]. Available: http://ieeexplore.ieee.org/stamp/stamp.jsp?arnumber=7038151.

[15] M. Couraud, Cattaert D, Paclet F, Oudeyer P, and Rugy A, "Model and experiments to optimize co-adaptation in a simplified myoelectric control system," *J. Neural Eng.*, 2017, Accessed: Feb. 20, 2018. [Online]. Available: http://iopscience.iop.org/article/10.1088/1741-2552/aa87cf/pdf.

[16] C. H. Nguyen, G. K. Karavas, and P. Artemiadis, "Adaptive multi-degree of freedom Brain Computer Interface using online feedback: Towards novel methods and metrics of mutual adaptation between humans and machines for BCI," *PLoS One*, vol. 14, no. 3, p. e0212620, 2019, doi: 10.1371/journal.pone.0212620.

[17] J. S. Müller, C. Vidaurre, M. Schreuder, F. C. Meinecke, P. Von Bünau, and K. R. Müller, "A mathematical model for the two-learners problem," *J. Neural Eng.*, vol. 14, no. 3, 2017, doi: 10.1088/1741-2552/aa620b.

[18] S. Cheamanunkul and Y. Freund, "Co-adaptation in a Handwriting Recognition System," 2014. Accessed: Nov. 21, 2018. [Online]. Available: https://arxiv.org/pdf/1409.2897.pdf.

[19] F. Lotte, C. Jeunet, J. Mladenovic, B. N. ' Kaoua, and L. Pillette, "A BCI challenge for the signal processing community: considering the user in the loop," 2018. Accessed: Oct. 07, 2018. [Online]. Available: https://hal.inria.fr/hal-01762573v2.

[20] A. Abu-Rmileh, E. Zakkay, L. Shmuelof, and O. Shriki, "Co-adaptive Training

Improves Efficacy of a Multi-Day EEG-Based Motor Imagery BCI Training," *Front. Hum. Neurosci.*, vol. 13, no. October, pp. 1–8, 2019, doi: 10.3389/fnhum.2019.00362.

[21] "Coapt, LLC." https://www.coaptengineering.com/ (accessed Aug. 19, 2020).

[22] A. D. Roche, H. Rehbaum, D. Farina, and O. C. Aszmann, "Prosthetic Myoelectric Control Strategies: A Clinical Perspective," *Curr. Surg. Reports*, vol. 2, no. 3, p. 44, 2014, doi: 10.1007/s40137-013-0044-8.

[23] J. M. Hahne, "Machine Learning Based Myoelectric Control," Berlin Institute of Technology, 2016.

[24] A. J. Young, L. H. Smith, E. J. Rouse, and L. J. Hargrove, "Classification of simultaneous movements using surface EMG pattern recognition," *IEEE Trans. Biomed. Eng.*, vol. 60, no. 5, pp. 1250–1258, 2013, doi: 10.1109/TBME.2012.2232293.

[25] Y. Teh, R. B. Woodward, and L. J. Hargrove, "Comparing the Effects of Signal Noise on Pattern Recognition and Linear Regression-Based Myoelectric Controllers," *Proc. Annu. Int. Conf. IEEE Eng. Med. Biol. Soc. EMBS*, vol. 2018-July, pp. 2132–2135, 2018, doi: 10.1109/EMBC.2018.8512693.

[26] J. Hahne *et al.*, "Linear and nonlinear regression techniques for simultaneous and proportional myoelectric control," *IEEE Trans. Neural Syst. Rehabil. Eng.*, vol. 22, no. 2, pp. 269–279, 2014, doi: 10.1109/TNSRE.2014.2305520.

[27] A. Fougner, Ø. Stavdahl, P. J. Kyberd, Y. G. Losier, P. A. Parker, and S. Member, "Control of Upper Limb Prostheses : Terminology and Proportional Myoelectric Control — A Review," vol. 20, no. 5, pp. 663–677, 2012.

[28] N. Jiang, S. Dosen, K. R. Muller, and D. Farina, “Myoelectric Control of Artificial Limbs: Is There a Need to Change Focus? [In the Spotlight],” *IEEE Signal Process. Mag.*, vol. 29, no. 5, pp. 150–152, 2012, doi: 10.1109/msp.2012.2203480.

[29] H. J. Hwang, J. M. Hahne, and K. R. Müller, “Real-time robustness evaluation of regression based myoelectric control against arm position change and donning/doffing,” *PLoS One*, vol. 12, no. 11, pp. 1–22, 2017, doi: 10.1371/journal.pone.0186318.

[30] A. W. Shehata, E. J. Scheme, and J. W. Sensinger, “Evaluating internal model strength and performance of myoelectric prosthesis control strategies,” *IEEE Trans. Neural Syst. Rehabil. Eng.*, vol. 26, no. 5, pp. 1046–1055, 2018, doi: 10.1109/TNSRE.2018.2826981.

[31] A. W. Shehata, E. J. Scheme, and J. W. Sensinger, “The effect of myoelectric prosthesis control strategies and feedback level on adaptation rate for a target acquisition task,” *2017 Int. Conf. Rehabil. Robot.*, pp. 200–204, 2017, doi: 10.1109/ICORR.2017.8009246.

[32] S. Zhai and P. Milgram, “Human performance evaluation of manipulation schemes in virtual environments,” *Proc. IEEE Virtual Real. Annu. Int. Symp.*, pp. 155–161, 1993, doi: 10.1109/VRAIS.1993.380784.

[33] C. Igual, J. Igual, J. M. Hahne, and L. C. Parra, “Adaptive auto-regressive proportional myoelectric control,” *IEEE Trans. Neural Syst. Rehabil. Eng.*, vol. PP, no. JANUARY, pp. 1–1, 2019, doi: 10.1109/TNSRE.2019.2894464.

[34] A. Ameri, E. N. Kamavuako, E. J. Scheme, K. B. Englehart, and P. A. Parker, “Real-time, simultaneous myoelectric control using visual target-based training

paradigm," *Biomed. Signal Process. Control*, vol. 13, pp. 8–14, 2014, doi: 10.1016/j.bspc.2014.03.006.

[35] A. Ameri, E. Kamavuako, E. Scheme, K. Englehart, and P. Parker, "Support Vector Regression for Improved Real Time, Simultaneous Myoelectric Control," *TNSRE*, 2013, doi: 10.1109/TNSRE.2014.2323576.

[36] W. Won Kim, F. Tendick, S. Ellis, and L. Stark, "A comparison of position and rate control for telemanipulations with consideration of manipulator system dynamics," *IEEE J. Robot. Autom.*, vol. 3, no. 5, pp. 426–436, Oct. 1987, doi: 10.1109/JRA.1987.1087117.

[37] B. Hudgins, P. Parker, and R. N. Scott, "A New Strategy for Multifunction Myoelectric Control," *IEEE Trans. Biomed. Eng.*, vol. 40, no. 1, pp. 82–94, 1993, doi: 10.1109/10.204774.

[38] V. Gregori, A. Gijsberts, and B. Caputo, "Adaptive learning to speed-up control of prosthetic hands: A few things everybody should know," *IEEE Int. Conf. Rehabil. Robot.*, pp. 1130–1135, 2017, doi: 10.1109/ICORR.2017.8009401.

[39] W. Guo, X. Sheng, J. Liu, L. Hua, D. Zhang, and X. Zhu, "Towards zero training for myoelectric control based on a wearable wireless sEMG armband," *IEEE/ASME Int. Conf. Adv. Intell. Mechatronics, AIM*, vol. 2015-Augus, pp. 196–201, 2015, doi: 10.1109/AIM.2015.7222531.

[40] F. Lotte *et al.*, "A review of classification algorithms for EEG-based brain-computer interfaces: A 10 year update," *J. Neural Eng.*, vol. 15, no. 3, 2018, doi: 10.1088/1741-2552/aab2f2.

[41] Y. Zhang, Z. Wang, and Z. Zhang, "Comparison of Online Adaptive Learning

Algorithms for Myoelectric Hand Control," pp. 69–75, 2016.

[42] M. R. Tuga, R. Rupp, D. Liebetanz, R. Mikut, and M. Reischl, "Concept of a Co-Adaptive Training Environment for Human-Machine Interfaces Based on EMG-Control," *Biomed. Eng. / Biomed. Tech.*, vol. 58, p. Suppl1, 2013, doi: 10.1515/bmt-2013-4388.

[43] C. Igual, L. A. Pardo, J. M. Hahne, and J. Igual, "Myoelectric control for upper limb prostheses," *Electron.*, vol. 8, no. 11, pp. 1–21, 2019, doi: 10.3390/electronics8111244.

[44] O. Fukuda, T. Tsuji, M. Kaneko, and A. Otsuka, "A human-assisting manipulator teleoperated by EMG signals and arm motions," *IEEE Trans. Robot. Autom.*, vol. 19, no. 2, pp. 210–222, 2003, doi: 10.1109/TRA.2003.808873.

[45] J. Liu, "Adaptive myoelectric pattern recognition toward improved multifunctional prosthesis control," *Med. Eng. Phys.*, vol. 37, no. 4, pp. 424–430, 2015, doi: 10.1016/j.medengphy.2015.02.005.

[46] O. Fukuda, T. Tsuji, M. Kaneko, and A. Otsuka, "A human-assisting manipulator teleoperated by EMG signals and arm motions," *IEEE Trans. Robot. Autom.*, vol. 19, no. 2, pp. 210–222, 2003, doi: 10.1109/TRA.2003.808873.

[47] J. He, D. Zhang, X. Sheng, and X. Zhu, "A comparison of open-loop and closed-loop adaptive calibration for pattern recognition based myoelectric control," *Proc. Annu. Int. Conf. IEEE Eng. Med. Biol. Soc. EMBS*, vol. 2015-Novem, pp. 1144–1147, 2015, doi: 10.1109/EMBC.2015.7318568.

[48] Y. Fang, D. Zhou, K. Li, and H. Liu, "Interface Prostheses with Classifier-Feedback based User Training," *IEEE Trans. Biomed. Eng.*, pp. 1–1, 2016, doi:

10.1109/TBME.2016.2641584.

[49] M. Markovic, M. A. Schweisfurth, L. F. Engels, D. Farina, and S. Dosen, "Myocontrol is closed-loop control: Incidental feedback is sufficient for scaling the prosthesis force in routine grasping," *J. Neuroeng. Rehabil.*, vol. 15, no. 1, 2018, doi: 10.1186/s12984-018-0422-7.

[50] J. W. Sensinger and S. Dosen, "A Review of Sensory Feedback in Upper-Limb Prostheses From the Perspective of Human Motor Control," *Front. Neurosci.*, vol. 14, 2020, doi: 10.3389/fnins.2020.00345.

[51] D. S. Childress, "Closed-loop control in prosthetic systems: Historical perspective," *Ann. Biomed. Eng.*, vol. 8, no. 4–6, pp. 293–303, 1980, doi: 10.1007/BF02363433.

[52] S. Dosen, M. Markovic, K. Somer, B. Graimann, and D. Farina, "EMG Biofeedback for online predictive control of grasping force in a myoelectric prosthesis," *J. Neuroeng. Rehabil.*, vol. 12, no. 1, 2015, doi: 10.1186/s12984-015-0047-z.

[53] I. Saunders and S. Vijayakumar, "The role of feed-forward and feedback processes for closed-loop prosthesis control," *J. Neuroeng. Rehabil.*, vol. 8, no. 1, p. 60, 2011, doi: 10.1186/1743-0003-8-60.

[54] T. Pistohl, C. Cipriani, A. Jackson, and K. Nazarpour, "Abstract and proportional myoelectric control for multi-fingered hand prostheses," *Ann. Biomed. Eng.*, vol. 41, no. 12, pp. 2687–2698, 2013, doi: 10.1007/s10439-013-0876-5.

[55] M. Ison, I. Vujaklija, B. Whitsell, D. Farina, and P. Artemiadis, "High-Density Electromyography and Motor Skill Learning for Robust Long-Term Control of a

7-DoF Robot Arm," *IEEE Trans. Neural Syst. Rehabil. Eng.*, vol. 24, no. 4, pp. 424–433, 2016, doi: 10.1109/TNSRE.2015.2417775.

[56] A. W. Shehata, L. F. Engels, M. Controzzi, C. Cipriani, E. J. Scheme, and J. W. Sensinger, "Improving Internal Model Strength and Performance of Prosthetic Hands Using Augmented Feedback," *J. Neuroeng. Rehabil.*, vol. 15, no. 70, 2018, doi: https://doi.org/10.1186/s12984-018-0417-4.

[57] Q. H. Mach, M. D. Hunter, and R. S. Grewal, "Neurophysiological correlates in interface design: An HCI perspective," *Comput. Human Behav.*, vol. 26, no. 3, pp. 371–376, 2010, Accessed: Jul. 16, 2020. [Online]. Available: https://www.academia.edu/13707967/Neurophysiological_correlates_in_interface_design_An_HCI_perspective.

[58] J. P. Cunningham *et al.*, "A closed-loop human simulator for investigating the role of feedback control in brain-machine interfaces," *J Neuro-physiol*, vol. 105, pp. 1932–1949, 2011, doi: 10.1152/jn.00503.2010.

[59] K. Nazarpour, A. Barnard, and A. Jackson, "Flexible cortical control of task-specific muscle synergies," *J. Neurosci.*, vol. 32, no. 36, pp. 12349–12360, Sep. 2012, doi: 10.1523/JNEUROSCI.5481-11.2012.

[60] C. W. Antuvan, M. Ison, and P. Artemiadis, "Embedded human control of robots using myoelectric interfaces," *IEEE Trans. Neural Syst. Rehabil. Eng.*, vol. 22, no. 4, pp. 820–827, 2014, doi: 10.1109/TNSRE.2014.2302212.

[61] S. Dangi, S. Gowda, R. Heliot, and J. M. Carmena, "Adaptive Kalman filtering for closed-loop Brain-Machine Interface systems," *2011 5th Int. IEEE/EMBS Conf. Neural Eng. NER 2011*, pp. 609–612, 2011, doi: 10.1109/NER.2011.5910622.

[62] S. M. Radhakrishnan, S. N. Baker, and A. Jackson, “Learning a Novel Myoelectric-Controlled Interface Task,” *J. Neurophysiol.*, vol. 100, no. 4, pp. 2397–2408, 2008, doi: 10.1152/jn.90614.2008.

[63] R. Héliot, K. Ganguly, J. Jimenez, and J. M. Carmena, “Learning in closed-loop brainmachine interfaces: Modeling and experimental validation,” *IEEE Trans. Syst. Man, Cybern. Part B Cybern.*, vol. 40, no. 5, pp. 1387–1397, 2010, doi: 10.1109/TSMCB.2009.2036931.

[64] D. Blustein, A. Shehata, K. Englehart, and J. Sensinger, “Conventional analysis of trial-by-trial adaptation is biased: Empirical and theoretical support using a Bayesian estimator,” *PLoS Comput. Biol.*, vol. 14, no. 12, pp. 1–15, 2018, doi: 10.1371/journal.pcbi.1006501.

[65] C. W. Antuvan, M. Ison, and P. Artemiadis, “Embedded human control of robots using myoelectric interfaces,” *IEEE Trans. Neural Syst. Rehabil. Eng.*, vol. 22, no. 4, pp. 820–827, 2014, doi: 10.1109/TNSRE.2014.2302212.

[66] M. Ison, C. W. Antuvan, and P. Artemiadis, “Learning efficient control of robots using myoelectric interfaces,” *Proc. - IEEE Int. Conf. Robot. Autom.*, pp. 2880–2885, 2014, doi: 10.1109/ICRA.2014.6907273.

[67] J. He, D. Zhang, N. Jiang, X. Sheng, D. Farina, and X. Zhu, “User adaptation in long - term , open - loop myoelectric training : implications for EMG pattern recognition in prosthesis control,” *J. neural*, 2015, doi: 10.1088/1741-2560/12/4/046005.

[68] J. Merel, D. M. Pianto, J. P. Cunningham, and L. Paninski, “Encoder-Decoder Optimization for Brain-Computer Interfaces,” *PLoS Comput. Biol.*, vol. 11, no. 6,

2015, doi: 10.1371/journal.pcbi.1004288.

[69] C. Vidaurre, C. Sannelli, K.-R. Müller, and B. Blankertz, "Machine-Learning-Based Coadaptive Calibration for Brain-Computer Interfaces," *Neural Comput.*, vol. 23, no. 3, pp. 791–816, 2011, doi: 10.1162/NECO_a_00089.

[70] S. Dangi *et al.*, "Design and Analysis of Closed-Loop Decoder Adaptation Algorithms for Brain-Machine Interfaces," 2013. Accessed: Oct. 28, 2018. [Online]. Available: https://www.mitpressjournals.org/doi/pdf/10.1162/NECO_a_00460.

[71] I. M. Rezazadeh, M. Firoozabadi, H. Hu, and S. M. R. H. Golpayegani, "Co-adaptive and affective human-machine interface for improving training performances of virtual myoelectric forearm prosthesis," *IEEE Trans. Affect. Comput.*, vol. 3, no. 3, pp. 285–297, 2012, doi: 10.1109/T-AFFC.2012.3.

[72] J. Merel, D. M. Pianto, J. P. Cunningham, and L. Paninski, "Encoder-Decoder Optimization for Brain-Computer Interfaces," *PLoS Comput. Biol.*, vol. 11, no. 6, p. 1004288, 2015, doi: 10.1371/journal.pcbi.1004288.

[73] C. Igual, J. Igual, J. M. Hahne, and L. C. Parra, "Adaptive auto-regressive proportional myoelectric control," *IEEE Trans. Neural Syst. Rehabil. Eng.*, vol. PP, no. JANUARY, p. 1, 2019, doi: 10.1109/TNSRE.2019.2894464.

[74] Y. Zhang and M. S. Chase, "A control-theoretic approach to brain-computer interface design," 2016. Accessed: Jun. 09, 2019. [Online]. Available: http://www.cnbc.cmu.edu/~schase/docs/zhang_acc_2016.pdf.

[75] J. Merel, R. Fox, T. Jebara, and L. Paninski, "A multi-agent control framework for co-adaptation in brain-computer interfaces," 2013. Accessed: Sep. 17, 2018.

[Online]. Available: http://papers.nips.cc/paper/5176-a-multi-agent-control-framework-for-co-adaptation-in-brain-computer-interfaces.

[76] S. Strogatz, M. Friedman, A. J. Mallinckrodt, and S. McKay, "Nonlinear Dynamics and Chaos: With Applications to Physics, Biology, Chemistry, and Engineering," *Computers in Physics*, vol. 8, no. 5. p. 532, 1994, doi: 10.1063/1.4823332.

[77] E. N. Lorenz, "Deterministic Nonperiodic Flow," *J. Atmos. Sci.*, vol. 20, 1963.

[78] "Chaos Theory and Meteorological Predictions | Encyclopedia.com." https://www.encyclopedia.com/environment/energy-government-and-defense-magazines/chaos-theory-and-meteorological-predictions (accessed Jul. 09, 2020).

[79] M. Brennan, M. Palaniswami, and P. Kamen, "Do Existing Measures of Poincare Plot Geometry Reflect Nonlinear Features of Heart Rate Variability?," *IEEE Trans. Biomed. Eng.*, vol. 48, no. 11, pp. 1342–1347, 2001.

[80] G. Teschl, *Ordinary Differential Equations and Dynamical Systems*, no. 140. American Mathematical Society, 2012.

[81] M. R. Roussel, "Maps and differential equations," vol. 3, pp. 1–26, 2005, doi: 10.4171/022-3/1.

[82] S. Mukherjee, S. K. Palit, and D. K. Bhattacharya, "Approximate discrete dynamics of EMG signal," *Appl. Math. Comput.*, vol. 243, pp. 879–888, 2014, doi: 10.1016/j.amc.2014.06.059.

[83] H. Bassily, M. Daqaq, and J. Wagner, "Application of Pseudo-Poincaré Maps to Assess Gas Turbine System Health," pp. 1–23.

[84] K. Khalil, "Nonlinear Systems Third Edition."

[85] D. Chelidze, "Bifurcations and Poincaré Maps." Accessed: Nov. 23, 2020.

[Online]. Available: https://personal.egr.uri.edu/chelidz/documents/mce567_Chapter_6.pdf.

[86] M. Rezaei, H. Mohammadi, and H. Khazaie, "EEG/EOG/EMG data from a cross sectional study on psychophysiological insomnia and normal sleep subjects," *Data Br.*, vol. 15, pp. 314–319, 2017, doi: 10.1016/j.dib.2017.09.033.

[87] A. K. Golińska, "Poincaré plots in analysis of selected biomedical signals," *Stud. Logic, Gramm. Rhetor.*, vol. 35, no. 48, pp. 117–127, Dec. 2013, doi: 10.2478/slgr-2013-0031.

[88] C. K. Karmakar, A. H. Khandoker, J. Gubbi, and M. Palaniswami, "Complex correlation measure: a novel descriptor for Poincaré plot.," *Biomed. Eng. Online*, vol. 8, p. 17, 2009, doi: 10.1186/1475-925X-8-17.

[89] A. Tabor, S. Bateman, E. Scheme, D. R. Flatla, and K. Gerling, "Designing game-based myoelectric prosthesis training," *Conf. Hum. Factors Comput. Syst. - Proc.*, vol. 2017-May, pp. 1352–1363, 2017, doi: 10.1145/3025453.3025676.

[90] P. M. Fitts, "The Information Capacity of the Human Motor System in Controlling the Amplitude of Movement 1," *J. Exp. Psychol.*, vol. 47, no. 6, 1954, Accessed: Jul. 31, 2018. [Online]. Available: http://www2.psychology.uiowa.edu/faculty/mordkoff/InfoProc/pdfs/Fitts 1954.pdf.

[91] E. J. Scheme and K. B. Englehart, "Validation of a selective ensemble-based classification scheme for myoelectric control using a three-dimensional fitts' law test," *IEEE Trans. Neural Syst. Rehabil. Eng.*, vol. 21, no. 4, pp. 616–623, 2013, doi: 10.1109/TNSRE.2012.2226189.

[92] E. Scheme and K. Englehart, “A flexible user interface for rapid prototyping of advanced real-time myoelectric control schemes,” 2008. Accessed: Sep. 20, 2018. [Online]. Available: https://dukespace.lib.duke.edu/dspace/bitstream/handle/10161/2810/Scheme 2008.pdf;sequence=3.

[93] R. W.-J. of Physiology-London and undefined 1963, “A method of measuring motor unit activity in human muscle,” *CAMBRIDGE UNIV Press 40 …*.

[94] L. H. Smith, L. J. Hargrove, B. A. Lock, and T. A. Kuiken, “Determining the optimal window length for pattern recognition-based myoelectric control: balancing the competing effects of classification error and controller delay NIH Public Access,” *IEEE Trans Neural Syst Rehabil Eng*, vol. 19, no. 2, pp. 186–192, 2011, doi: 10.1109/TNSRE.2010.2100828.

[95] E. J. Earley, L. J. Hargrove, and T. A. Kuiken, “Dual window pattern recognition classifier for improved partial-hand prosthesis control,” *Front. Neurosci.*, vol. 10, no. FEB, Feb. 2016, doi: 10.3389/fnins.2016.00058.

[96] G. Casiez, N. Roussel, and D. Vogel, “1€ Filter: A Simple Speed-based Low-pass Filter for Noisy Input in Interactive Systems,” *Proc. 2012 ACM Annu. Conf. Hum. Factors Comput. Syst. - CHI ’12*, p. 2527, 2012, doi: 10.1145/2207676.2208639.

[97] M. P. Tulppo, T. H. Makikallio, T. E. S. Takala, T. Seppanen, and H. V Huikuri, “Quantitative beat-to-beat Analysis of Heart Rate Dynamics During Exercise,” *Am. Physiol. Soc.*, pp. 244–252, 1996.

[98] W. Tucker, “Computing accurate Poincaré maps,” 2002.

[99] I. S. MacKenzie, “Fitts’ Law as a Research and Design Tool in Human-Computer

Interaction," *Human–Computer Interaction*, vol. 7, no. 1. pp. 91–139, 1992, doi: 10.1207/s15327051hci0701_3.

[100] N. E. Bunderson and T. A. Kuiken, "Quantification of feature space changes with experience during electromyogram pattern recognition control," *IEEE Trans. Neural Syst. Rehabil. Eng.*, vol. 20, no. 3, pp. 239–246, 2012, doi: 10.1109/TNSRE.2011.2182525.

[101] A. Radmand, E. Scheme, and K. Englehart, "A characterization of the effect of limb position on EMG features to guide the development of effective prosthetic control schemes," *2014 36th Annu. Int. Conf. IEEE Eng. Med. Biol. Soc. EMBC 2014*, pp. 662–667, 2014, doi: 10.1109/EMBC.2014.6943678.

[102] R. L. Smith *et al.*, "Analyzing heart rate variability in infants using non-linear Poincaré techniques," *Comput. Cardiol.*, vol. 36, pp. 673–676, 2009.

[103] T. Biala, M. Dodge, F. S. Schlindwein, and M. Wailoo, "Heart rate variability using Poincaré plots in 10 year old healthy and intrauterine growth restricted children with reference to maternal smoking habits during pregnancy," *Comput. Cardiol. (2010).*, vol. 37, pp. 971–974, 2010.

[104] K. Hayase, K. Hayashi, and T. Sawa, "Hierarchical Poincaré analysis for anaesthesia monitoring," *J. Clin. Monit. Comput.*, vol. 34, no. 6, pp. 1321–1330, 2020, doi: 10.1007/s10877-019-00447-0.

[105] K. Hayashi, N. Mukai, and T. Sawa, "Poincaré analysis of the electroencephalogram during sevoflurane anesthesia," *Clin. Neurophysiol.*, vol. 126, no. 2, pp. 404–411, 2015, doi: 10.1016/j.clinph.2014.04.019.

[106] L. van Dijk, C. K. van der Sluis, H. W. van Dijk, and R. M. Bongers, "Learning an

EMG Controlled Game: Task-Specific Adaptations and Transfer.," *PLoS One*, vol. 11, no. 8, p. e0160817, 2016, doi: 10.1371/journal.pone.0160817.

[107] R. B. Stein and M. Walley, "Functional comparison of upper extremity amputees using myoelectric and conventional prostheses.," *Arch. Phys. Med. Rehabil.*, vol. 64, no. 6, pp. 243–8, Jun. 1983, Accessed: Feb. 11, 2019. [Online]. Available: http://www.ncbi.nlm.nih.gov/pubmed/6860093.

[108] Y. Zhang and S. M. Chase, "Recasting brain-machine interface design from a physical control system perspective," *J Comput Neurosci*, vol. 39, pp. 107–118, 2015, doi: 10.1007/s10827-015-0566-4.

[109] Z. Danziger, A. Fishbach, and F. A. Mussa-Ivaldi, "Learning algorithms for human-machine interfaces," *IEEE Trans. Biomed. Eng.*, vol. 56, no. 5, pp. 1502–1511, 2009, doi: 10.1109/TBME.2009.2013822.

[110] P. Cisek, "Internal Models," vol. 70, no. 4. pp. 787–801, 2009, doi: 10.1016/j.neuron.2011.04.012.Rethinking.

[111] A. Krasoulis, S. Vijayakumar, and K. Nazarpour, "Evaluation of regression methods for the continuous decoding of finger movement from surface EMG and accelerometry," *Int. IEEE/EMBS Conf. Neural Eng. NER*, vol. 2015-July, pp. 631–634, 2015, doi: 10.1109/NER.2015.7146702.

Appendix: Supplementary Results

The following results confirm the findings from Chapter 4.

7.1 Separability Index (SI)

The user's ability to separate classes of motion in EMG control can be used as a measure of the robustness of the pattern recognition scheme.

7.1.1 Time Series Analysis

The time series plot with the best-fit line of the subjects' SI over the 10 days using four protocol combinations is shown in Fig. 7-1. An improvement in all three subjects' SI is seen in Fig. 7-1a and 7-1c when the participants performed with the non-adapting protocols. A steeper positive slope can be noted on the subjects' best-fit lines when the protocol called for a sparsely trained algorithm ($\bar{A}S$), indicating more attainable separability in their motions when the system trained with fewer target-distance data. We can generally note the increase in oscillations in SI values when the adapting algorithm is used, representing a lack of separability in the users' actions.

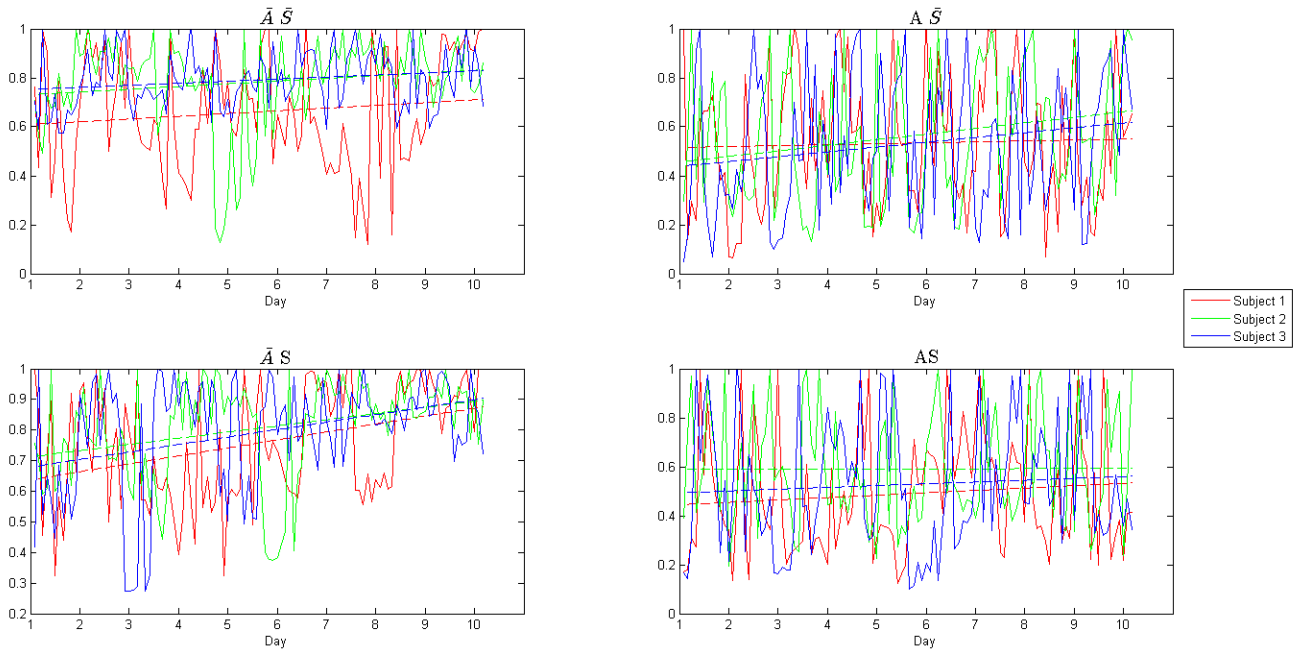

Figure 6-1: Time Series plot of three subjects' SI values, 10 days, 4 protocol combinations. Dotted lines represent line of best fit.

7.1.2 Poincaré Mapping

The observed results from the Poincaré map of S1's SI values (Fig. 7-2) corroborate the results observed from the time series plot (Fig. 7-1). There is more variability in the SI values when the subject uses the adapting algorithm (Fig. 7-2b, 7-2d) than the non-adapting algorithm (Fig. 7-2a, c). However, additional to this observation, we can pinpoint that there was greater variation in S1's SI values when the algorithm trained on the full data-set (Fig. 7-2a) than the sparsely trained dataset (Fig. 7-2c). This variation is mainly apparent at the beginning of the $\overline{AS}$ sessions but the amount of variability reduces as the number of days increase, leading to S1's highest SI values on their last day.

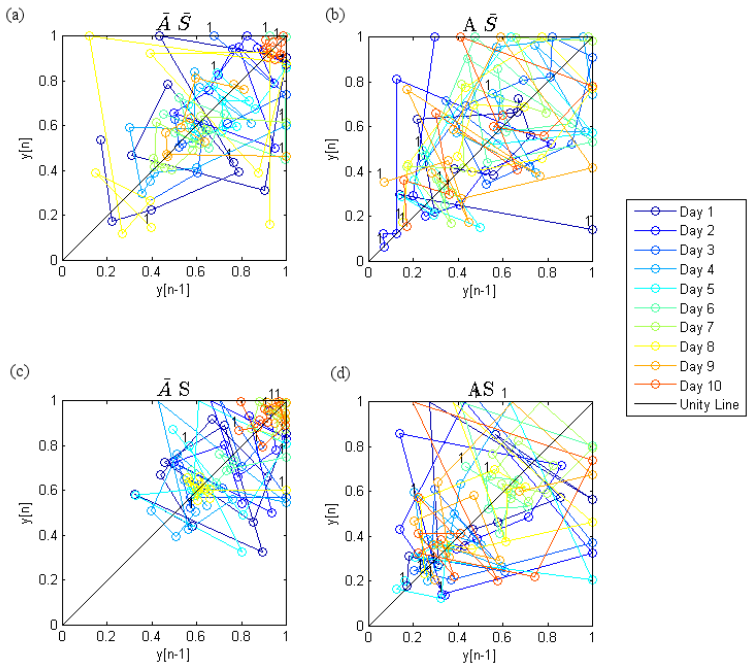

Figure 6-2: Poincaré of S1's SI values, 10 days, 4 protocol combinations

Similarly, S3 confirms the findings from the time series plot. For conciseness, only S3 is represented to provide a sample of a Poincaré map of SI values by an experienced subject in EMG control, seen in Fig. 7-3. SI values are more varied across the unity line when the algorithm adapts, suggesting uncertainty in the user's control, even after 10 days. Conversely, when the algorithm is non-adapting, the user's SI values are consistent and concentrated, seen in Fig. 4-11a. An improvement in SI values over the 10 days can be seen in Fig. 7-3c ($A\bar{S}$), agreeing with the information provided in the time series plot.

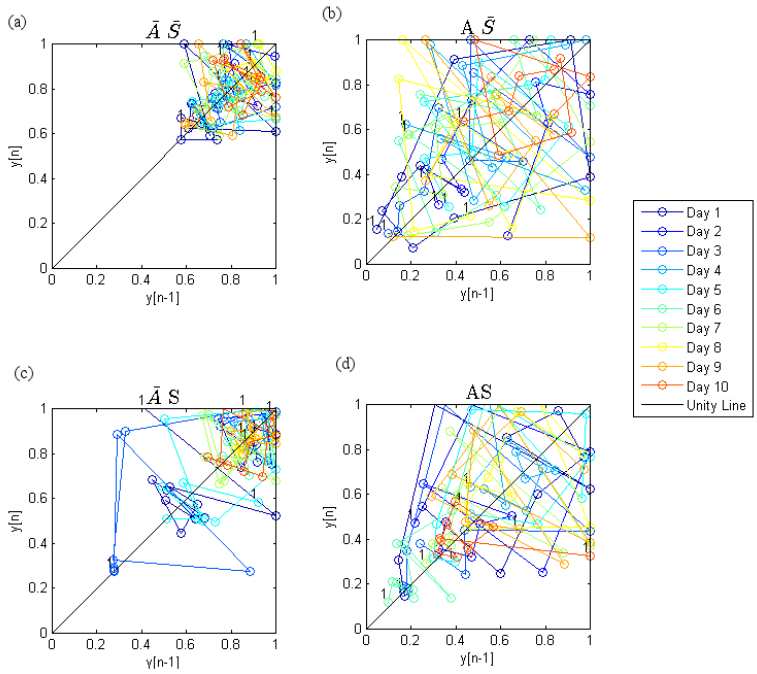

Figure 6-3: Poincaré map of S3's SI values, 10 days, 4 protocol combinations

7.1.3 Learning Analysis

Through the time series and Poincaré plots, we can see an improvement in SI values over the 10-day experiment when the algorithm did not adapt. However, looking at the Poincaré clusters and applying knowledge based on their location and behaviour around the unity line, we can say that users attempted to learn their EMG control more when the algorithm was adapting to their actions after every set than when it was static. This inference is made from the wide range of SI values along the unity line, representing learning. The information provided by the Poincaré map can lead to developments in the training stages of co-adaptive HMIs to understand whether a longer training period is required to improve the user's performance as they adapted slowly to their system.

Visually, the time series and Poincaré maps of the SI values show more oscillations when subjects used adapting protocols than non-adapting protocols. The Poincaré maps of the adapting algorithm protocols resemble a mixture of the simulated spiral and oscillatory stochastic Poincaré maps in Table 3-3. These stochastic oscillatory and spiral behaviours are also seen in the Poincaré maps relating SI values from non-adaptive protocol combinations. However, the seemingly random changes in values as they oscillate between each set do not appear to devalue the performance of the user's EMG control, seen by the relatively high SI values.

Empirically, the SD ratios calculated from the Poincaré graphs provide insight into the variability of the co-adaptive system (Fig. 7-4) as data across the protocol combinations and subjects are quite similar. The SD values are also indicative of a chaotic system, comparing these to the simulated chaotic system in Table 3-4. The adapting, sparsely-trained system (AS) has a slightly higher ratio than other protocol combinations, implying greater variation in separability within the daily sessions. However, the overall similarity in SD ratio values suggests an equal amount of learning and variation during the daily sessions for each subject's SI data. This result agrees with the information provided by the graphs of the time series and Poincaré, in that the co-adaptive system's separability progressed over time but did so chaotically.

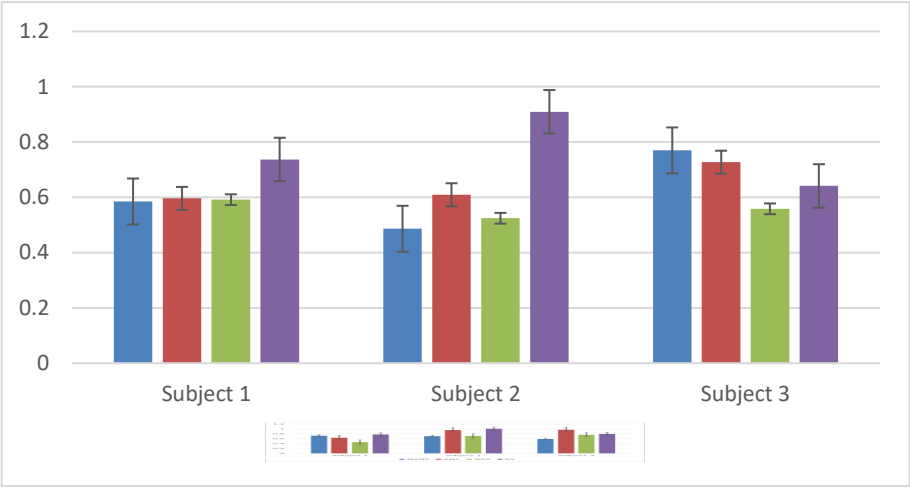

Figure 6-4: SD ratio calculated from the Poincaré map of the SI values of three subjects, 10 days, 4 protocol combinations

7.2 Regression Monitoring

The dynamics of the regressor were observed through time series and Poincaré plots of the median of the first PCA component of each set in the Feedback-Enabled and Testing stages. This measurement, henceforth called regression monitoring, observes the effects that parameter changes have on the trend and dynamics of the regressor.

7.2.1 Time Series Analysis

The time series of the regression monitoring metric was plotted the regression models in DOF 1 (Fig. 7-5) and DOF 2 (Fig. 7-6). We observe that the regressor performed worse as days increased during the non-adapting, sparsely trained ($\bar{A}S$) protocol for both DOFs. Most of the regression models in the protocols in Fig. 7-5 and show a decrease in performance, but as these plots represent the median of a PCA coefficient, their value does not provide valuable insight.

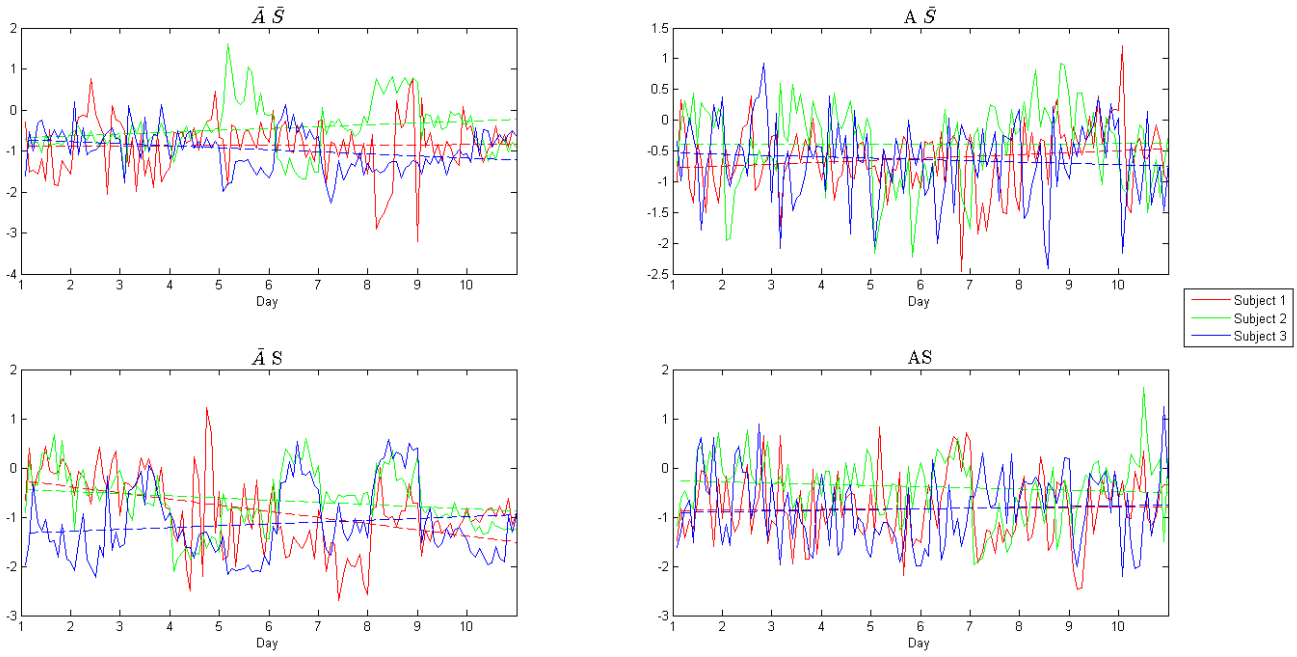

Figure 6-5: Time series plot of three subjects' Regression Monitoring metric, DOF 1, 10 days, 4 protocol combinations. Dotted lines represent line of best fit.

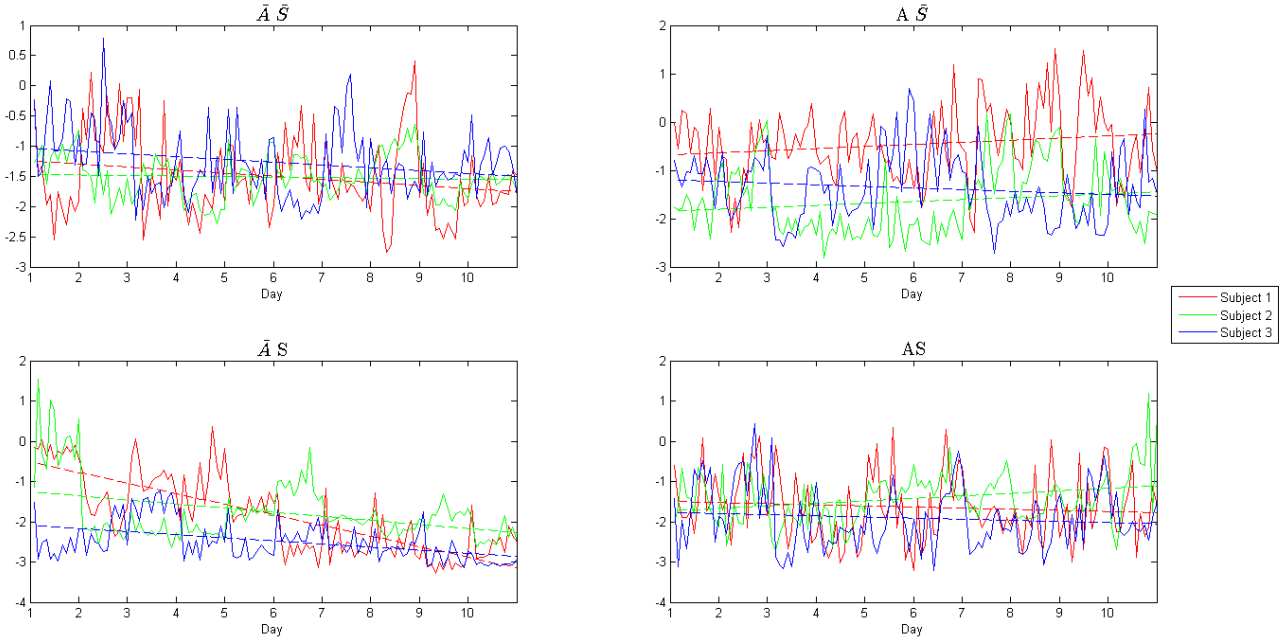

Figure 6-6: Time series plot of three subjects' Regression Monitoring metric, DOF 2, 10 days, 4 protocol combinations. Dotted lines represent line of best fit.

7.2.2 Poincaré Mapping

Rather than focusing on the values of the Regression Monitoring metric, we can focus on the trend and dynamics of the regressor over the 10-day experiment by using Poincaré maps. Only plots comparing S1 and S3 are shown below, to compare regressor behaviour dependant on the users' experience in EMG control. Fig. 7-7 compares the two subjects' DOF 1 performance using the non-adapting, non-sparsely trained protocol ($\overline{AS}$) and the adapting, non-sparsely trained protocol ($A\bar{S}$). This comparison focuses on the algorithm adaptation and subject EMG control experience level. The regression monitoring metric in S3's $\overline{AS}$ sessions (Fig. 7-7b) follows the unity line more tightly than the other subplot cases, suggesting consistency in this regression model in each session over the 10 days. However, even with this apparent consistency, the DOF 1 regressor in both subjects' $\overline{AS}$ and $A\bar{S}$ sessions seem to be chaotic within the confines of a bounded area.

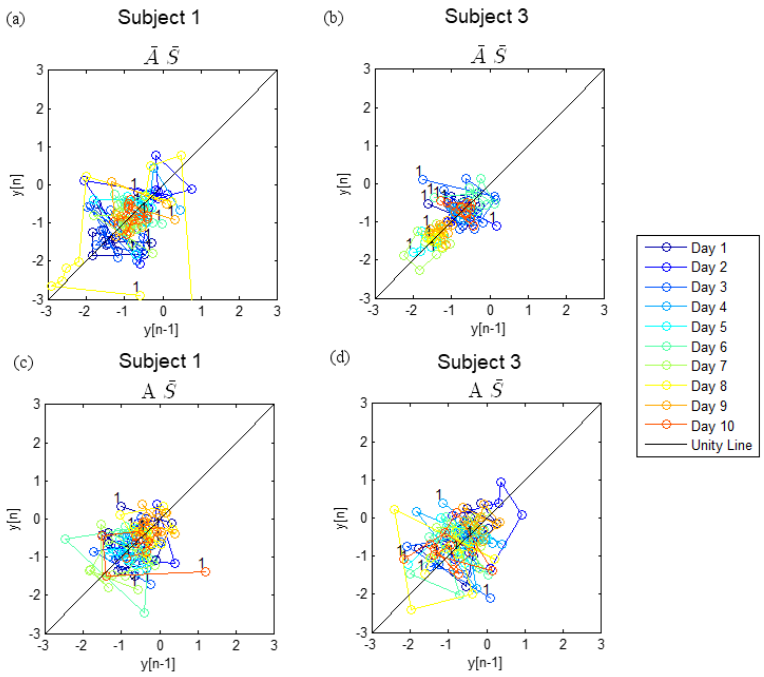

Figure 6-7: Poincaré map comparing the regression monitoring metric from S1 and S3's DOF 1 performance using the $\overline{AS}$ and $A\bar{S}$ protocol, 10 days

The regression monitoring metric from the subjects' DOF 2 model is compared in Fig. 7-8 for the $\bar{A}S$ and AS protocols. In these plots, the regressor trends downwards along the unity line as the number of days in the experiment increases. This downward motion is more precise when the algorithm is non-adapting and when the user has more experience (Fig. 7-8b). Algorithm adaptation leads to more variation across the unity line in the regressor's behaviour, as seen in Fig. 7-8c and 7-8d.

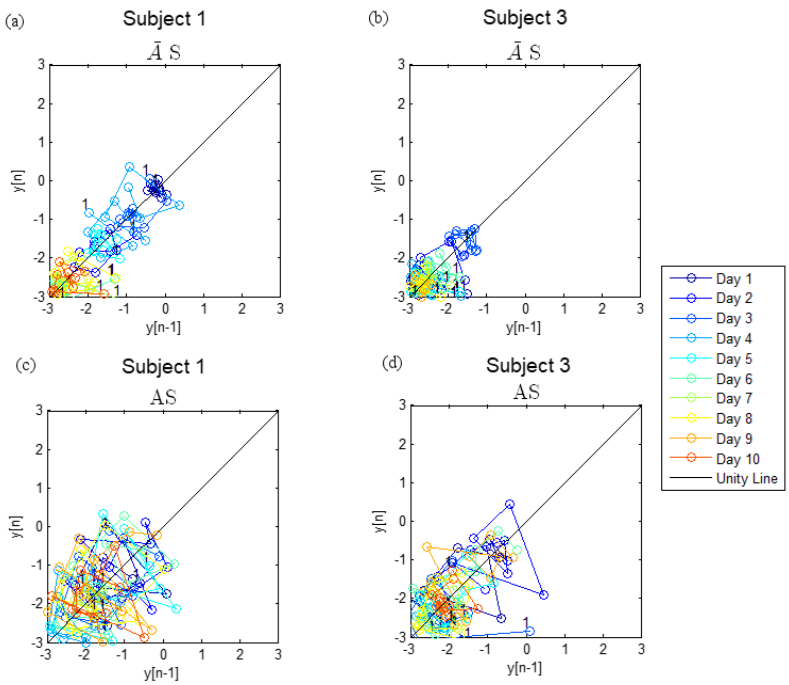

Figure 6-8: Poincaré map comparing the regression monitoring metric of S1 and S3's DOF 2 performance during the $\bar{A}S$ and AS protocol, 10 days

7.2.3 Learning Analysis

The Regressor Monitoring metric focuses on the regressor's adaptation and any learning effect observed through this metric would signify a regressor change. A learning effect is noted through Poincaré maps by the length of data along the unity line, i.e. the major axis. In our results, the regression monitoring metric's range along the unity line was similar for all protocol combinations and subjects, signifying a lack of learning from the regressor. The time series plot also provided little evidence of a learning effect as most of the linear best-fit lines had little to no slope. The proposition that there was no learning is based on visual tools, and empirical evidence may be required to further investigate.

Quantitative analysis was used to determine whether there was a learning effect present in the regressor, or whether variability in the chaotic system prevented any

improvement. The SD ratio values (Fig. 7-9) were relatively high, suggesting high amounts of variance across the unity line with comparable growth along the unity line. The short-term to long-term variability in the co-adaptive system is particularly high when S1 used the $\overline{AS}$ protocol.

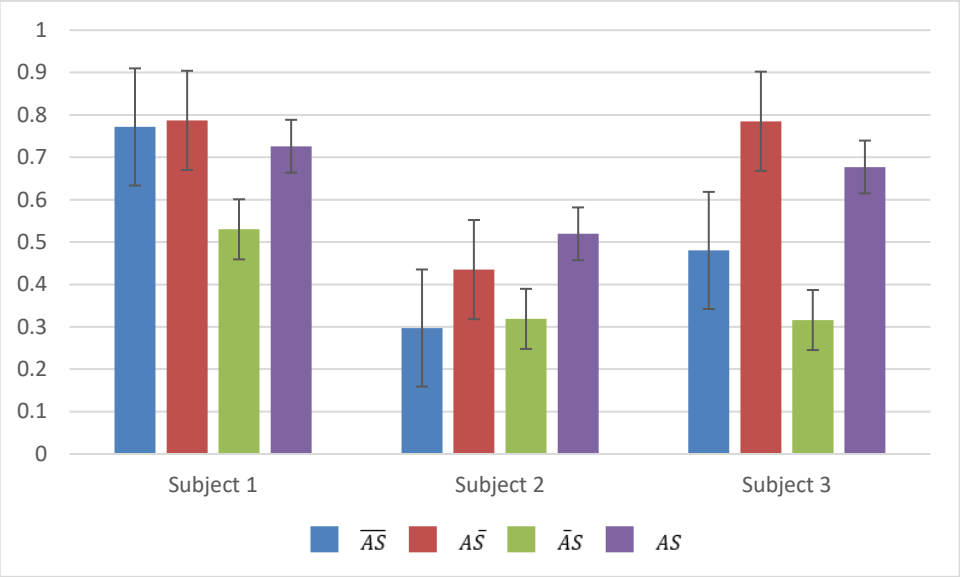

Figure 6-9: SD ratio values of the Poincaré maps of the regression monitoring metric, DOF 1, taken from three subjects, 10 days, 4 protocol combinations

The dynamics of the co-adaptive system were further investigated through SD2 values. Fig. 7-10 shows the SD2 values, representing the learning effect over 10 days, of the DOF 1 regression monitoring metric. The similarity between the SD2 values in Fig. 7-10 shows that the behaviour of the co-adaptive system along the unity line did not depend on any of the protocol combination changes. Fig. 7-9 and 7-10 corroborate the finding that apparent randomness in the behaviour of the system is high in adapting protocols, independent of the experience of the user.

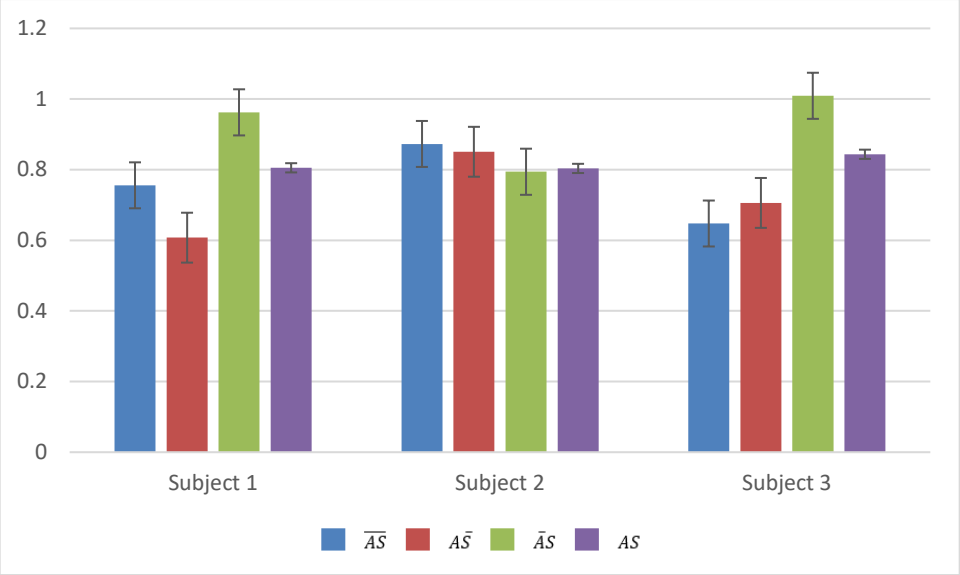

Figure 6-10: SD2 values of the Poincaré maps of the regression monitoring metric, DOF 1, taken from three subjects, 10 days, 4 protocol combinations

7.3 Repeatability Index: S2

S2 shows improvement when the system is non-adapting and fully trained ($A\bar{S}$). When the algorithm is adapting and trained on the full dataset ($\overline{AS}$, Fig. 7-11a), S2's ability to be repeatable decreases over time, highlighting the effect that machine adaptation has on the user's EMG control.

Fig. 7-11 shows S2's RI values plotted on a Poincaré map over the 10 days. Recall that S2's time series plot was the most informative of the three subjects. When the algorithm was non-adapting, in Fig. 7-11 a and c, S2's repeatability indices fluctuated between high and low values along the unity line, ending the experiment with scores lower than achieved throughout the experiment. Particularly interesting is the wide range of RI values seen in Fig. 7-11b ($A\bar{S}$), suggesting that the user was not very repeatable in their contractions. Yet the lack of variability across the unity line suggests that there was no

uncertainty in the user's control, rather the user explored their abilities as the algorithm adapted over the 10 days.

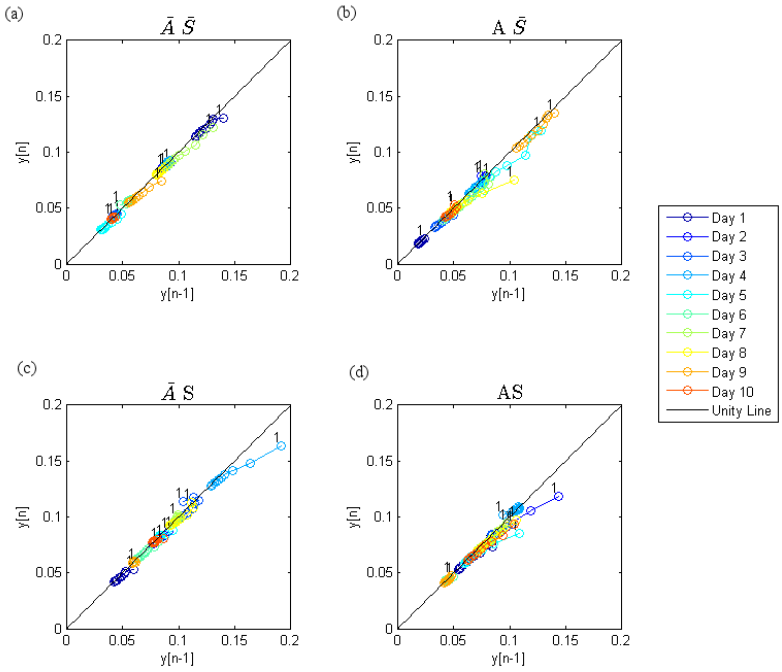

Figure 6-11: Poincaré map of S2's RI values, 10 days, 4 protocol combinations

Curriculum Vitae

Candidate's full name: Ishtar Al-Tahir

Universities attended (with dates and degrees obtained):

University of New Brunswick (BSc. in Electrical and Computer Engineering, 2017)

Publications: None

Conference Presentations: None